NASA TECHNICAL NOTE

NASA TN D-6619

INVESTIGATION OF SONIC BOOM GENERATED BY THIN, NONLIFTING, RECTANGULAR WINGS

by Sanford S. Davis

Ames Research Center
Moffett Field, Calif. 94035

NATIONAL AERONAUTICS AND SPACE ADMINISTRATION • WASHINGTON, D. C. • DECEMBER 1971

1. Report No.	2. Government Accession No.	3. Recipient's Catalog No.
NASA TN D-6619		

4. Title and Subtitle	5. Report Date
INVESTIGATION OF SONIC BOOM GENERATED BY THIN, NONLIFTING, RECTANGULAR WINGS	December 1971
	6. Performing Organization Code
7. Author(s)	8. Performing Organization Report No.
Sanford S. Davis	A-4109
	10. Work Unit No.
9. Performing Organization Name and Address	136-13-02-00-21
NASA Ames Research Center Moffett Field, Calif., 94035	11. Contract or Grant No.
	13. Type of Report and Period Covered
12. Sponsoring Agency Name and Address	Technical Note
National Aeronautics and Space Administration Washington, D. C. 20546	14. Sponsoring Agency Code

15. Supplementary Notes

16. Abstract

A new theory is described for predicting sonic boom pressure signatures emitted by nonlifting rectangular wings. Comparisons are made with previous (Whitham) theory and with experimentally determined near field signatures. Although both theories agree with experiment for low aspect ratio wings, Whitham's theory seriously overpredicts signature length for high aspect ratio wings. No experiments were conducted in the far field, but the two theories predict nearly identical results in this region.

17. Key Words (Suggested by Author(s))	18. Distribution Statement
Shock waves Supersonic flight Sonic booms Noise (sound)	Unclassified -- Unlimited

19. Security Classif. (of this report)	20. Security Classif. (of this page)	21. No. of Pages	22. Price*
Unclassified	Unclassified	44	$3.00

*For sale by the National Technical Information Service, Springfield, Virginia 22151

SYMBOLS

d	streamwise scale distance (1/2 chord)
$f(r_i)$	function which identifies characteristic family
$G(\xi_i, r_i, p_i)$	difference between linearized and corrected shock location
ℓ	span of wing
m	slope of wing airfoil section at the leading edge
M	free-stream Mach number
p_∞	free-stream static pressure
p_{SH}	pressure just upstream of the shock wave
R	distance from axis of symmetry of wing, $\sqrt{\left(y - \frac{\ell}{2}\right)^2 + z^2}$
$\overline{R}(t)$	radius of equivalent body of revolution
$S(t)$	cross-sectional area distribution of equivalent body of revolution
u	perturbation velocity in free-stream direction
u_{r_i}	perturbation velocity in direction of increasing r_i
V	free-stream velocity
x,y,z	Cartesian coordinate system
x_1, y_1	variables of integration
β	$\sqrt{M^2 - 1}$
γ	ratio of specific heats, $\frac{c_p}{c_v}$
Δp	difference between local and static pressure
θ	auxiliary angle, $\pi - p_2$ (fig. 2)
ξ_o	family of characteristics that contribute to the shock wave
ξ_1, r_1, p_1	transformed coordinate system in $z > 0$, $0 < y < \ell$
ξ_2, r_2, p_2	transformed coordinate system in $z > 0$, $y < 0$

Φ linearized perturbation velocity potential

ϕ asymptotic approximation to ϕ for $\frac{\xi_i}{r_i} \to 0$

Subscript

i i = 1, coordinate system $0 < y < \ell$, $z > 0$; i = 2, coordinate system $y < 0$, $z > 0$

INVESTIGATION OF SONIC BOOM GENERATED BY THIN, NONLIFTING, RECTANGULAR WINGS

Sanford S. Davis

Ames Research Center

SUMMARY

A new theory is described for predicting sonic boom pressure signatures emitted by nonlifting rectangular wings. Comparisons are made with previous (Whitham) theory and with experimentally determined near field signatures. Although both theories agree with experiment for low aspect ratio wings, Whitham's theory seriously overpredicts signature length for high aspect ratio wings. No experiments were conducted in the far field, but the two theories predict nearly identical results in this region.

INTRODUCTION

The standard methods used to predict the sonic boom are based on a theory developed by Whitham (refs. 1 and 2). Although the theory was originally devised for slender, axisymmetric configurations, Whitham extended his theory to include arbitrary configurations by using the methods of geometrical acoustics (ref. 3). He later realized that the procedures developed for slender, symmetrical bodies of revolution may be used intact for a nonsymmetrical configuration if the so-called equivalent body of revolution is introduced. But if the equivalent body of revolution is not slender, Whitham's theory as given in reference 2 is not strictly applicable. The extent to which the pressure signatures calculated for a nonslender equivalent body deviates from the experimentally determined signatures will be explored in this report.

In order to predict sonic boom pressure signatures more accurately in the nearfields and midfields for nonslender configurations, a new theory has been developed. Although restricted to nonlifting, rectangular wings, this theory predicts substantial differences in pressure signatures when compared with the equivalent body theory. The purpose of this report is to evaluate signatures predicted by both theories and to compare them with experimentally determined signatures.

The rectangular wing represents a very interesting model configuration because of the diversity of flows surrounding it. The wing tip Mach cones divide the flow into three distinct regions: (1) the two-dimensional region, (2) the tip-cone region, and (3) the interaction region. In the two-dimensional region, the flow is independent of the spanwise coordinate. The flow field is exactly the same as that generated by a two-dimensional wing

with the same airfoil section as the rectangular wing. The tip-cone region contains a three-dimensional flow, a small portion of which has conical symmetry. In the interaction region the flow is fully three-dimensional. Therefore, a theory that predicts the shock wave generated by a rectangular wing includes elements of the theories of conical flows, two- and three-dimensional flows, and the transition flows that separate these regions. It will be shown that the new theory, called the uniform theory, more correctly describes the flow in each of these regions.

The flow geometry and the uniform theory are reviewed briefly in the following sections. The theory is developed for a parabolic arc airfoil section, but the uniform theory can be applied to any wing with a biconvex airfoil section.

LINEAR FLOW FIELD GEOMETRY

Consider the wing to be fixed in an (x,y,z) Cartesian coordinate system. The mean plane of the wing occupies part of the x-y plane in the region $x > 0$, $y > 0$. A supersonic stream flows in the direction of increasing x at Mach number M. Since the flow is symmetric with respect to the plane $z = 0$, only the region $z > 0$ will be considered.

The thickness distribution of the wing is denoted by $t(x)$ and is given by the following formula:

$$\left.\begin{array}{lll} t(x) = 0 & \text{all } y & x \leqslant 0 \\ t(x) = 2m(x - x^2/2d) & 0 < y < \mathcal{l} & \\ t(x) = 0 & y < 0,\ y > \mathcal{l} & 0 \leqslant x \leqslant 2d \\ t(x) = 0 & \text{all } y & x \geqslant 2d \end{array}\right\} \qquad (1)$$

In equation (1) $\mathcal{l}$ represents the span of the wing, $2d$ is its chord, and m is the slope of the airfoil section at the leading edge. Figure 1 is a plan view of the wing.

A fundamental property of supersonic flows is the separation of the flow field into disturbed and undisturbed regions. In linearized theory, the boundary between these two regions is a characteristic surface (i.e., the wave front). For the rectangular wing, the linearized wave front consists of the following surface in $z > 0$.

1. The planar surface

$$x - \beta z = 0 \qquad 0 < y < \mathcal{l}$$

where

$$\beta^2 = M^2 - 1$$

2. A portion of the tip cone at (0, 0, 0)

$$x - \beta^2\sqrt{y^2 + z^2} = 0 \qquad y < 0$$

3. A portion of the tip cone at (0, ℓ, 0)

$$x - \beta\sqrt{(y - \ell)^2 + z^2} = 0 \qquad y > \ell$$

If the tip cones, given by 2 and 3 above, are extended to $y > 0$, $y < \ell$, three distinct disturbed regions are defined. These regions are denoted in figure 1 by the numerals I, II, and III. In region I the flow is two-dimensional, the same as for a wing of infinite span. In region II, inside one or the other of the tip cones, the flow is dependent on only one tip cone. Regions I and II alone represent the flow field for a semi-infinite wing. Region III is the interaction region. In this region the flow field is influenced by both tip cones. Region III represents the typical flow field pattern at large distances from a finite wing.

The general appearance of these regions, at various distances from the wing, is also shown in figure 1. In each of the sketches labeled nearfield, midfield, and farfield, the wave front is shown as it would appear when intersected by a plane at a constant value of x. In the nearfield sketch, which represents a distance downstream of one or two spans, regions I, II, and III are about the same size. In the midfield, at a few spans downstream, regions I and II are reduced at the expense of region III. Many spans downstream, the characteristic farfield pattern emerges. Region I becomes very small, region II becomes a crescent shaped area with a thickness the order of the span, while region III dominates the flow.

DESCRIPTION OF THE UNIFORM THEORY

The basis of the uniform theory is Whitham's hypothesis (as developed and applied in refs. 2 and 3), which states that linear theory gives a correct first approximation to variations of the physical quantities along the linearized (free-stream) characteristics, but the location of these linearized characteristics is in error. In order to apply Whitham's hypothesis to the rectangular wing, a better approximation to linearized theory must be obtained than the one afforded by the equivalent body method. Unfortunately, a better approximation cannot be expressed in the form of the Whitham F-function. Once this form of solution is abandoned, Whitham's simple and elegant results cannot be duplicated. But there is no reason why an improved form of the linear solution could not be used as the basis of a characteristic correction, and this in fact is the crux of the uniform theory. This theory will be described briefly in the following paragraphs.

An expression for the perturbation velocity potential due to the presence of a nonlifting rectangular wing in an otherwise undisturbed stream of Mach number M is

$$\Phi = -\frac{V}{\pi}\iint_A \frac{m(1 - x_1/d)dx_1dy_1}{\sqrt{(x - x_1)^2 - \beta^2(y - y_1)^2 - \beta^2z^2}} \tag{2}$$

In this expression $m(1 - x_1/d)$ represents the streamwise slope distribution of the parabolic airfoil, V is the free-stream velocity, and A is the area in the plane of the wing bounded by the Mach forecone from the field point (x,y,z), and the edges of the wing.

In the region $z > 0$, $0 < y < \ell$ a new set of coordinates based on the family of planar characteristics will be introduced. Let

$$x = \xi_1 + \beta r_1$$

$$y = p_1$$

$$z = r_1$$

If the location of the point P_1 in figure 2 is expressed in terms of (ξ_1, r_1, p_1), the potential can be written as

$$\Phi = -\frac{V}{\pi}\iint_A \frac{m(1 - x_1/d)dx_1dy_1}{\sqrt{X_1}} \tag{3}$$

$$X_1 = (\xi_1 - x_1)^2 + 2\beta r_1(\xi_1 - x_1) - \beta^2(p_1 - y_1)^2$$

In the region near the wave front, ξ_1 is always much smaller than r_1 (see fig. 2). Since only the region near the front is of interest, equation (3) may be simplified by neglecting the first term in the expression for X_1. If this quadratic term in $(\xi_1 - x_1)$ is neglected, the resulting expression for Φ is valid for small values of ξ_1/r_1. The simplified form of equation (3) is

$$\Phi \sim \phi = -\frac{V}{\pi}\iint_A \frac{m(1 - x_1/d)dx_1dy_1}{\sqrt{2\beta r_1(\xi_1 - x_1) - \beta^2(p_1 - y_1)^2}} \tag{4}$$

where A now represents the area in the plane of the wing bounded by

$$2\beta r_1(\xi_1 - x_1) - \beta^2(p_1 - y_1)^2 = 0$$

and the wing edges. Note that in this approximation the intersection of the plane of the wing and the Mach forecone is represented by an approximating

parabola instead of a hyperbola. (The F-function approach, by neglecting the quadratic term $\beta^2(p_1 - y_1)^2$, would represent this approximation by a straight line parallel to the leading edge.) Equation (4) represents the uniformly valid approximation to the linear perturbation potential in the region $z > 0$, $0 < y < \ell$.

Another set of coordinates is chosen in the region $z > 0$, $y < 0$. (The region $z > 0$, $y > \ell$ will not be examined since the plane $y = \ell/2$ represents a plane of symmetry.)

$$x = \xi_2 + \beta r_2$$

$$y = r_2 \cos p_2$$

$$z = r_2 \sin p_2$$

If the location of the point P_2 in figure 2 is expressed in terms of (ξ_2, r_2, p_2), the potential in this coordinate system is

$$\Phi = -\frac{V}{\pi} \iint_A \frac{m(1 - x_1/d)dx_1dy_1}{\sqrt{X_2}} \tag{5}$$

$$X_2 = (\xi_2 - x_1)^2 + 2\beta r_2(\xi_2 - x_1 + \beta y_1 \cos p_2) - \beta^2 y_1^2$$

Equation (5) can be approximated in the region where ξ_2/r_2 is small if the term $(\xi_2 - x_1)^2$ in X_2 is neglected. This approximate potential is written

$$\Phi \sim \phi = -\frac{V}{\pi} \iint_A \frac{m(1 - x_1/d)dx_1dy_1}{\sqrt{2\beta r_2(\xi_2 - x_1 + \beta y_1 \cos p_2) - \beta^2 y_1^2}} \tag{6}$$

where A represents the area in the plane of the wing bounded by

$$2\beta r_2(\xi_2 - x_1 + \beta y_1 \cos p_2) - \beta^2 y_1^2 = 0$$

and the wing edges. As mentioned above, this approximation results in a parabolic forecone intersection. (It does not give as crude an approximation as the F-function in which X_2 is linearized by neglecting $\beta^2 y_1^2$.) Equation (6) represents the uniformly valid approximation to the potential in the region $z > 0$, $y < 0$. It can be shown that this form of ϕ is a uniformly valid asymptotic representation to Φ with respect to the parameter p_2 as $\xi_2/r_2 \to 0$.

The choice of new coordinates in equations (4) and (6) is not arbitrary, but is closely related to the rays and wave fronts of geometrical acoustics. In this context, the x-axis plays the role of time and the y-z plane represents the space; r_1 and r_2 represent distance along a "ray"; p_1 and p_2 are ray labelling parameters; and ξ_1 and ξ_2 are "phase variables." Flow past a rectangular wing is analogous in many respects to diffraction of a pulse by a plane wall, and "shadow regions" or "reflected regions" may be defined in the y-z plane (e.g., region I is a reflected zone, region II is a shadow region and the shadow boundary is the ray $p_1 = 0$ or $p_2 = \pi/2$). This analogy has been very useful in determining the expressions (4) and (6).

The approximations (4) and (6) may be integrated directly, resulting in the following expressions for the axial perturbation velocity:

1. In the region $z > 0$, $0 < y < \ell$:

$$\left.\begin{aligned} \frac{u}{V} &= \frac{-m}{\pi\beta}\left[\left(1 - \frac{\xi_1}{d}\right)(\pi - \tan^{-1} A_o - \tan^{-1} A_\ell) - \frac{\beta p_1^2 A_o}{2dr_1} - \frac{\beta(\ell - p_1)^2 A_\ell}{2dr_1}\right] \\ A_o &= \mathrm{Re}\left(\frac{2\xi_1 r_1}{\beta p_1^2} - 1\right)^{1/2} \\ A_\ell &= \mathrm{Re}\left[\frac{2\xi_1 r_1}{\beta(\ell - p_1)^2} - 1\right]^{1/2} \end{aligned}\right\} \qquad (7)$$

2. In the region $z > 0$, $y < 0$:

$$\left.\begin{aligned} \frac{u}{V} &= \frac{-m}{\pi\beta}\left[\left(1 - \frac{\xi_2}{d} - \frac{\beta r_2 \cos^2\theta}{2d}\right)(\tan^{-1} B_o - \tan^{-1} B_\ell) \right. \\ &\qquad \left. + \frac{\beta r_2 \cos^2\theta B_o}{2d} - \frac{\beta(r_2 \cos\theta + \ell)^2}{2r_2 d} B_\ell\right] \\ B_o &= \mathrm{Re}\left(\frac{2\xi_2}{\beta r_2 \cos^2\theta}\right)^{1/2} \\ B_\ell &= \mathrm{Re}\left[\frac{(2\xi_2 r_2/\beta) - 2r_2\ell\cos\theta - \ell^2}{(r_2\cos\theta + \ell)^2}\right]^{1/2} \end{aligned}\right\} \qquad (8)$$

where $\theta = \pi - p_2$.

Note that equations (7) include a region where both A_o and A_ℓ vanish. The perturbation velocity in this region is the same that would exist for a two-dimensional flow in the x-z plane. As A_o and A_ℓ become real, the tip cones modify this two-dimensional region. At very large values of r_1, if $\xi_1 \neq 0$, the solution reduces to the form that would be obtained by equivalent body theory. Likewise the form given by equations (8) reduces to the equivalent body solution as $r_2 \to \infty$. (See the appendix for the equivalent body corresponding to this wing.)

Returning to Whitham's hypothesis, the linearized solution given by equations (7) and (8) must be corrected to account for cumulative nonlinear effects. The correction procedure is to redefine the lines $\xi_1 = x - \beta r_1$ and $\xi_2 = x - \beta r_2$ to be the next approximations to the exact characteristic lines. The slope of the next higher-order characteristic lines in the planes p_i = constant is

$$\frac{dx}{dr_i} = \beta + \frac{(\gamma + 1)M^4}{2\beta^2}\frac{u(\xi_i,r_i,p_i)}{V} - M^2\left[\beta\frac{u(\xi_i,r_i,p_i)}{V} + \frac{u_{r_i}(\xi_i,r_i,p_i)}{V}\right]$$

$$+ \text{terms of order}\left[\left(\frac{u}{V}\right)^2, \quad \left(\frac{u_{r_i}}{V}\right)^2, \quad \left(\frac{u}{V}\frac{u_{r_i}}{V}\right), \quad \text{etc.}\right] \tag{9}$$

where $i = 1$ for $z > 0$, $0 < y < \ell$ and $i = 2$ for $z > 0$, $y < 0$. In equation (9) u_{r_i}/V represents the velocity in the direction of increasing r_i and $\gamma = c_p/c_v$ is the ratio of specific heats. Since only a first-order characteristic correction is required, only the linear terms in the exact expression for the characteristics have been included in equation (9). In addition, the term $\beta(u/V) + (u_{r_i}/V)$ may be neglected because the curvature of the characteristic line is very small. (For planar families of characteristics $\beta(u/V) + (u_{r_i}/V)$ is identically zero.)

Equation (9) may be integrated, and, in analogy with the procedure developed by Whitham, the corrected characteristics may be expressed as

$$x = \beta r_i - G(\xi_i,r_i,p_i) + \xi_i$$

$$G(\xi_i,r_i,p_i) = -\frac{(\gamma + 1)M^4}{2\beta^2}\int_o^{r_i}\frac{u}{V}(\xi_i,t,p_i)dt \tag{10}$$

The function $G(\xi_i,r_i,p_i)$ is given explicitly as:

1. In the region $z > 0$, $0 < y < \ell$

$$G(\xi_1,r_1,p_1) = \frac{(\gamma+1)M^4 m}{2\beta^2\pi}\left[\left(1-\frac{\xi_1}{d}\right)\left(\pi r_1 - r_1\tan^{-1}A_o + \frac{\beta p_1^2 A_o}{2\xi_1} - r_1\tan^{-1}A_\ell + \frac{\beta(\ell-p_1)^2 A_\ell}{2\xi_1}\right) - \frac{\beta p_1^2}{d}(A_o - \tan^{-1}A_o) - \frac{\beta(\ell-p_1)^2}{d}(A_\ell - \tan^{-1}A_\ell)\right]$$

2. In the region $z > 0,\ y < 0$

$$G(\xi_2,r_2,\theta) = \frac{(\gamma+1)M^4 m}{2\beta^2\pi}\left(\left(1-\frac{\xi_2}{d}\right)\left\{r_2\tan^{-1}B_o + r_2 B_o - \frac{2\xi_2}{\beta\cos^2\theta}\tan^{-1}B_o^{-1} - r_2\tan^{-1}B_\ell - \frac{r_2\cos\theta+\ell}{\cos\theta}B_\ell + \frac{2\xi_2}{\beta\cos^2\theta} + \tan^{-1}\left[\frac{\beta\cos\theta(r_2\cos\theta+\ell)}{2\xi_2-\beta\ell\cos\theta}B_\ell\right]\right\} - \beta\ell\frac{r_2\cos\theta+\ell}{d}B_\ell + \frac{\beta\ell^2}{d}\tan^{-1}\left[\frac{(r_2\cos\theta+\ell)B_\ell}{\ell}\right] - \frac{\beta r_2^2\cos^2\theta}{4d}\tan^{-1}B_o + \frac{\beta r_2^2\cos^2\theta}{4d}B_o + \frac{\beta r_2^2\cos^2\theta}{4d}B_o^3 - \frac{\beta r_2^2\cos^2\theta}{4d}B_o^4\tan^{-1}B_o^{-1} + \frac{\beta r_2^2\cos^2\theta}{4d}\tan^{-1}B_\ell + \frac{\beta^2\ell^2\cos\theta(r_2\cos\theta+\ell)}{8d(\xi_2-\beta\ell\cos\theta)}B_\ell - \frac{\xi_2(2\xi_2-\beta\ell\cos\theta)(r_2\cos\theta+\ell)}{4d\cos\theta(\xi_2-\beta\ell\cos\theta)}B_\ell - \frac{\beta^2\cos\theta(r_2\cos\theta+\ell)^3}{8d(\xi-\beta\ell\cos\theta)}B_\ell^3 + \frac{\beta r_2^2\cos^2\theta}{4d}B_o^4\tan^{-1}\left[\frac{\beta\cos\theta(r_2\cos\theta+\ell)}{2\xi_2-\beta\ell\cos\theta}B_\ell\right]\right)$$

Equations (7), with ξ_1 given by equation (10) represent the uniformly valid first-order expression for the velocity field in the region $z > 0,\ 0 < y < \ell$. Equations (8), with ξ_2 given by equation (10), represent the analogous result for $z > 0,\ y < 0$.

The solutions represented by equations (7) and (10, i=1) or equations (8) and (10, i=2) are multivalued, and thus do not represent a physically plausible situation. In order to eliminate the multivalues, a shock wave must be introduced into the flow field. The shock wave separates the regions of disturbed and undisturbed flow, and is located by the rule that the direction of the shock wave bisects the angle between the characteristics which meet at a point.

In the undisturbed flow, the slope of the characteristic is the free-stream wave slope β. In the disturbed flow, the characteristic direction to be used is associated with the family that carries local discontinuities in the perturbation quantities. In the case of the shock produced by a rectangular wing, more than one such family exists. For example, figure 3 shows the distorted characteristics in the plane of symmetry of the wing. (In the plane of symmetry ($p_1 = \ell/2$) both tip cones have the same trace.) In the region ahead of the trace of the distorted tip cone characteristic, the family of distorted planar characteristics is used to calculate the shock direction. But within the influence domain of the tip cone, the family associated with the tip cone trace is used to determine the shock-wave slope.

Each family of characteristics may be expressed as

$$\xi_o = \xi_i - f(r_i)$$

where ξ_o identifies the family to be used in the bisection rule, and $f(r_i)$ is a function appropriate to each family. In figure 3, where $i = 1$, the two families used are (1) $\xi_o = \xi_1$, $f(r_1) = 0$ and (2) $\xi_o = \xi_1 - \beta(\ell/2)^2/2r_1$, $f(r_1) = \beta(\ell/2)^2/2r_1$.

In terms of the parameter ξ_o, the corrected characteristics can be expressed as

$$x = \beta r_i - G[\xi_o + f(r_i), r_i] + \xi_o + f(r_i) \tag{11}$$

The bisection rule, when applied to (11), becomes

$$\left.\begin{aligned} \text{Slope of shock} &= \frac{1}{2}\left[(\beta) + \left(\beta - \frac{\partial G}{\partial r_i} + \frac{\partial f}{\partial r_i}\right)\right] \\ \text{Slope of shock} &= \beta - \frac{1}{2}\frac{\partial G}{\partial r_i} + \frac{1}{2}\frac{\partial f}{\partial r_i} \end{aligned}\right\} \tag{12}$$

If the position of the shock wave is given by

$$x_{sh} = \beta r_i - H(r_i) \tag{13}$$

then the slope of the shock dx_{sh}/dr_i is

$$\frac{dx_{sh}}{dr_i} = \beta - \frac{dH(r_i)}{dr_i} \tag{14}$$

or

$$\frac{dH}{dr_i} = \frac{1}{2}\frac{\partial G}{\partial r_i} - \frac{1}{2}\frac{\partial f}{\partial r_i} \tag{15}$$

Note that all partial derivatives in equation (15) are to be taken with ξ_o held constant.

From equations (11) and (13), H may be expressed as

$$H = G - \xi_o - f \tag{16}$$

Equations (15) and (16) represent a first-order, nonlinear, ordinary differential equation for ξ_o as a function of r_i. The functional form of G is so complicated that a numerical approach must be used to solve this equation.

In order to solve equations (15) and (16) a modification of the familiar Euler-Cauchy forward integration procedure was used. In terms of small, finite increments the differential system can be written as:

$$\frac{\Delta H}{\Delta r_i} = \frac{1}{2}\frac{\partial G}{\partial r_i} - \frac{1}{2}\frac{\partial f}{\partial r_i} \tag{17a}$$

$$\Delta H = \Delta G - \Delta\xi_o - \Delta f \tag{17b}$$

If starting values ξ_{oo} and r_{io} are chosen, and an increment Δr_i is given, equation (17a) shows that H changes by an amount

$$\Delta H = \left(\frac{1}{2}\frac{\partial G}{\partial r_i} - \frac{1}{2}\frac{\partial f}{\partial r_i}\right)\Bigg|_{\xi_{oo}, r_{io}} \Delta r_i \tag{18a}$$

When $r_i = r_{io} + \Delta r_i, \xi_o$ must change to $\xi_{oo} + \Delta\xi_o$. Equation (17b) reflects these increments as a change in ΔH by an amount

$$\Delta H = G(\xi_{oo} + \Delta\xi_o, r_{io} + \Delta r_i) - G(\xi_{oo}, r_{io}) - \Delta\xi_o - f(r_{io} + \Delta r_i) + f(r_{io}) \tag{18b}$$

Since H is the same in both equations (18a) and (18b),

$$\left.\frac{1}{2}\frac{\partial G}{\partial r_i} - \frac{1}{2}\frac{\partial f}{\partial r_i}\right|_{\xi_{oo},r_{io}} \Delta r_i = G(\xi_{oo} + \Delta\xi_o, r_{io} + \Delta r_i) - G(\xi_{oo}, r_{io}) - \Delta\xi_o$$

$$- f(r_{io} + \Delta r_i) + f(r_{io}) \qquad (19)$$

Equation (19) is a nonlinear algebraic equation for determining the unknown increment $\Delta\xi_o$. Once $\Delta\xi_o$ is found, a new starting point

$$\xi_o = \xi_{oo} + \Delta\xi_o, r_i = r_{io} + \Delta r_i$$

is found. The procedure is continued in this manner until the shock wave intersects a new family of characteristics. At this point ξ_o is redefined, the starting value of r_o is obtained from the preceding shock wave calculation, and the numerical integration can be restarted.

A slight difficulty in the procedure appears in the region $z > 0$, $y < 0$. For the starting values, $\xi_o = 0$, $r_2 = 0$ when substituted into the governing formulas, gives a result which is the indeterminate from 0/0. This problem is easily surmounted by matching to a conical flow solution near $r_2 = 0$.

Once the uniformly valid velocity field (with shock waves) has been obtained, the pressure rise at any point in the flow is calculated from the expression

$$\frac{\Delta p}{p_\infty} = -\gamma M^2 \frac{u}{V}$$

TEST PROCEDURES AND RESULTS

The general arrangement of the wing model is shown in figure 4. The symmetric airfoil section is a portion of a parabolic arc with a thickness distribution given by $t = 0.250\ (x - 0.197\ x^2)$ cm where t is the total thickness of the wing and x is a streamwise variable. Wings were fabricated with spans of 2.54 cm ($\ell/d = 1$), 10.16 cm ($\ell/d = 4$) and 15.24 cm ($\ell/d = 6$).

The experiments were conducted in the Ames 2- by 2-Foot Transonic Wind Tunnel at a Mach number of 1.40, a total pressure of 67.5 kN/m^2 and a total temperature 296° K. The arrangement of the model in the wind tunnel is shown in figure 5. The wing is supported in the test section by a tapered, conical sting faired into the wing's axis of symmetry. In order to minimize its effect on the front shock wave, the sting was fastened to the aft portion of the wing only. The 58.5 cm long sting assembly was secured to a linear actuator. The actuator had a continuously variable 15.24 cm streamwise motion,

and could be preset to any streamwise station prior to a test run. During a run, the x (streamwise) position of the wing was monitored by a calibrated potentiometer that was coupled to the 15.24 cm motion.

The shock-wave signature was measured with a slender 1° semiangle probe. The probe was offset 10.2 cm from the test section wall in order to exclude the effect of the wall's boundary layer from the measurements. On a plane inclined at 45° to the flow direction, four holes of 0.1024 cm diameter were drilled 7.62 cm from the probe tip. The pressures from this probe were measured relative to the free-stream static pressure by means of a calibrated pressure transducer.

Before each run, the wing was set in the test section so that the shock wave would be slightly behind the probe orifice. During the run the model was moved upstream in discrete steps by using the 15.24 cm motion of the actuator. At each step, the overpressure and distance moved was recorded. In this manner the entire shock-wave signature was obtained.

The results of the test program are summarized in figures 6 through 8. In each case the signatures are shown as normalized overpressures as a function of a horizontal scale measured from the position of the linearized leading Mach line. In all the figures, linear dimensions have been scaled with respect to the distance from the leading edge to the point of maximum thickness (i.e., with respect to 2.54 cm).

Figure 6 shows the shock-wave signatures for each of the three wings tested at varying distances below the wing (z direction). The wings having values of ℓ/d of 4 and 6 show strong two-dimensional shock waves in the near field, while the $\ell/d = 1$ wing shows a relatively weaker three-dimensional type of shock wave signature at all distances. The relative change in peak shock overpressure with distance is greatest for the wings with ℓ/d of 4 and 6. This effect is attributed to the sharp pressure relief associated with the wing tip cones. This behavior is indicated in figure 7(a) which shows the shock signature for the wing $\ell/d = 4$ and $z/d = 2.2$, but at different spanwise stations. The shock strength below the wing tip (span station $y/d = 0.0$) is about half the value at the centerline (span station $y/d = 2.0$) because the centerline station is in a two-dimensional flow field (as far as the shock strength is concerned), while the tip station is located within the dependence domain of the tip cone at $y/d = 0.0$. This ratio of 2:1 in peak overpressure is also predicted by the linearized theory, but (of course) the magnitudes obtained from linear theory are incorrect. At larger distances, the effect of spanwise variation is reduced. This lateral smoothing of the pressure field is due to the net cancelling effect of both wing tip cones on the two-dimensional field. This effect is shown in figure 7(b).

The influence of roll angle on the measured pressure signatures is shown in figure 8 for each of the three wings. In each case, the roll angle is defined by a rotation of the plane of the wing relative to the original horizontal plane about the axis of symmetry of the wing. (This axis is also the axis of the sting.) Distance from the axis of symmetry is denoted by R/d, where

$$\frac{R}{d} = \sqrt{\left(\frac{y}{d} - \frac{1}{2}\frac{\ell}{d}\right)^2 + \left(\frac{z}{d}\right)^2}$$

For the $\ell/d = 1$ wing, the signature is almost axisymmetric at $R/d = 16.0$ because at this distance the dominant effect on the sonic boom for this low aspect ratio wing is an axial source distribution. For the other wings large differences in meridional shock strengths and locations are apparent.

COMPARISON OF MEASUREMENTS AND THEORY

Predicted signatures of the uniform theory and equivalent body of revolution theory are compared with experimental signatures in figures 9 to 11. Details of the equivalent body theory for this configuration are described in the appendix. The signatures in the plane of symmetry below the wing for various length ratios, ℓ/d, are compared in figure 9. These signatures indicate that for short wings (i.e., $\ell/d = 1$, fig. 9(a)) both the uniform theory and the equivalent body theory predict the experimental results quite well at all the distance ratios shown. However, the signatures corresponding to longer wings (i.e., figs. 9(b) and 9(c)) indicate that while the equivalent body theory gives reasonable values for the peak overpressure, it substantially overestimates the signature length. On the other hand, with one exception, the uniform theory gives a better prediction for both the peak pressure and signature length for all values of ℓ/d. The case $z/d = 4$ in figure 9(b) is an exception because the tip-cone interaction has not been predicted exactly. This local defect has little effect on the overpressure at greater distances. The experimental signatures for $z/d = 8.0$ and 16.0 (fig. 9(c)) are probably less accurate than the others because the larger wing vibrated quite visibly during the test. These vibrations would tend to distort the signatures at the larger distance ratios. An indication of this distortion is the rapid expansion behind the shock wave for the case $z/d = 16.0$ as compared to that for $z/d = 8.0$. All previous experimental and theoretical results indicate that the slope of the curve in the expansion region decreases, rather than increases, in a regularly decaying shock wave signature.

In the midfield and farfield regions no experimental results are available, but a comparison of the two theories in their prediction of the peak overpressures is shown in figure 10. For $\ell/d = 1$, the agreement is good at all distances. For $\ell/d = 4$ and $\ell/d = 6$, the two theories lose mutual agreement at short distances. The nearfield experimental peak overpressures are also shown in figure 10, and these show that except for the one point corresponding to the $\ell/d = 6$ wing, good agreement between the uniform theory and experiment is achieved.

An important property of the decay curves shown in figure 10 is the behavior of the uniform theory curve for the higher span wings. These curves approach the equivalent body theory from below and show that some benefit may

be obtained by using this "non F-function" behavior in the midfield region. Further work on this point is necessary before any conclusions concerning the benefits of an unswept wing may be reached.

So far only the sonic boom overpressures under the wing have been compared. Figure 11 shows how the overpressures compare in the region to the side of the wing at $z/d = 16.0$. At this angle and distance, the uniform theory and the equivalent body theory predict similar signature shapes with reasonable agreement between theory and experiment.

CONCLUSIONS

A new theory for predicting sonic boom pressure signatures produced by nonlifting rectangular wings has been described and compared with the equivalent body of revolution theory and with a series of experimentally determined nearfield signatures. For low aspect ratio wings (i.e., less than one-half), both theories are in excellent agreement with experiment. For higher aspect ratio wings, with signatures taken in the vertical plane of symmetry, the equivalent body theory seriously overpredicts signature lengths. However, it does predict peak overpressure with accuracy comparable to the new theory. With signatures taken in the horizontal plane of the wing, the two theories are in excellent mutual agreement, and collectively are in reasonable agreement with experiment. Although no experiments were conducted in the farfield, the two theories give essentially identical predictions in this region.

Ames Research Center
National Aeronautics and Space Administration
Moffett Field, Calif., 94035, Sept. 2, 1971

APPENDIX

EQUIVALENT BODY METHOD

The equivalent body for a rectangular wing is different for each meridional angle θ. The proper form of the equivalent body can be obtained from equation (6) for the perturbation velocity potential. If the radical in equation (6) is linearized, the potential may be expressed as

$$\phi = -\frac{V}{\pi} \iint_A \frac{m(1 - x_1/d)dx_1\, dy_1}{\sqrt{2\beta r_2}\,\sqrt{\xi_2 - x_1 - \beta y_1 \cos\theta}} \tag{A1}$$

where A represents the area in the plane of the wing bounded by $\xi_2 - x_1 - \beta y_1 \cos\theta = 0$ and the wing boundary. An oblique coordinate system

$$\left.\begin{aligned} s_1 &= y_1 \\ t_1 &= x_1 + \beta y_1 \cos\theta \end{aligned}\right\} \tag{A2}$$

is introduced into equation (A1). In terms of (s_1,t_1) as variables of integration, the potential becomes

$$\phi = -\frac{V}{\pi\sqrt{2\beta r_2}} \int_o^{\xi_2} \frac{dt_1}{\sqrt{\xi_2 - t_1}} \left[\int_{wing} ds_1 m\left[1 - \frac{t_1}{d} + \left(\frac{\beta s_1}{d}\right)\cos\theta\right]\right] \tag{A3}$$

where the integral in the square bracket is taken over all values of s_1 on the wing.

From reference 2, the approximate perturbation velocity potential for a slender body of revolution may be expressed as

$$\phi = -\frac{V}{2\pi\sqrt{2\beta r_2}} \int_o^{\xi_2} dt_1 \frac{S'(t_1)}{\sqrt{\xi_2 - t_1}} \tag{A4}$$

where $S(t_1)$ is the cross-sectional area of the body at station t_1, and primes indicate differentiation with respect to t_1. A comparison of equations (A3) and (A4) shows that the disturbance field produced by the rectangular wing is the same as would exist for a slender body of revolution with a cross-sectional area distribution of

$$\frac{1}{2} S'(t_1) = \int_{\text{wing}} ds_1 m \left[1 - \frac{t_1}{d} + \left(\frac{\beta s_1}{d}\right) \cos \theta\right] \tag{A5}$$

Equation (A5) is valid for all values of t_1 less than 2d (i.e., excluding the influence domain of the trailing edge) and $S'(t_1)$ has the following representations in $0 < t_1 < 2d$.

$$S'(t_1) = \begin{cases} 2 \int_0^{t_1/\beta \cos \theta} ds_1 m \left[1 - \frac{t_1}{d} + \left(\frac{\beta s_1}{d}\right) \cos \theta\right] & t_1 < \beta \ell \cos \theta \\ 2 \int_0^{\ell} ds_1 m \left[1 - \frac{t_1}{d} + \left(\frac{\beta s_1}{d}\right) \cos \theta\right] & t_1 > \beta \ell \cos \theta \end{cases} \tag{A6}$$

Equation (A6) can be integrated to give an explicit formula for the cross-sectional area distribution of the equivalent slender body of revolution.

$$S(t_1) = \begin{cases} \dfrac{m \ell d}{\beta \frac{\ell}{d} \cos \theta} \left[\left(\frac{t_1}{d}\right)^2 - \frac{1}{3}\left(\frac{t_1}{d}\right)^3\right] & \dfrac{t_1}{d} < \beta \dfrac{\ell}{d} \cos \theta \\ m \ell d \left[2 \frac{t_1}{d} + \beta \frac{\ell}{d} \cos \theta \frac{t_1}{d} - \left(\frac{t_1}{d}\right)^2 \right. & \\ \left. - \beta \frac{\ell}{d} \cos \theta - \frac{1}{3}\left(\beta \frac{\ell}{d} \cos \theta\right)^2\right] & \dfrac{t_1}{d} > \beta \dfrac{\ell}{d} \cos \theta \end{cases} \tag{A7}$$

The radius distribution is given by $\bar{R}(t_1) = (1/\pi)\sqrt{S(t_1)}$.

Figure 12 shows a sampling of typical equivalent bodies of revolution for the wing $\ell/d = 4$. At $\theta = 0°$ and $\theta = 45°$ the equivalent bodies are slender, but at $\theta = 90°$ the equivalent body degenerates to a blunt forebody. Once these equivalent bodies have been found, the sonic boom corresponding to each of them may be found in a straightforward manner by following the procedures given in reference 2.

REFERENCES

1. Whitham, G. B.: The Behavior of Supersonic Flow Past a Body of Revolution Far From the Axis. Proceedings of the Royal Society of London, Series A, vol. 201, no. 1064, March 1950, pp. 89-109.

2. Whitham, G. B.: The Flow Pattern of a Supersonic Projectile. Commun. Pure and Appl. Math., vol. V, no. 3, Aug. 1952, pp. 301-348.

3. Whitham, G. B.: On the Propagation of Weak Shock Waves. J. Fluid Mech., vol. 1, part 3, Sept. 1956, pp. 290-318.

4. Friedlander, Friedrick G.: Sound Pulses. Cambridge University Press, Cambridge, Eng., 1958.

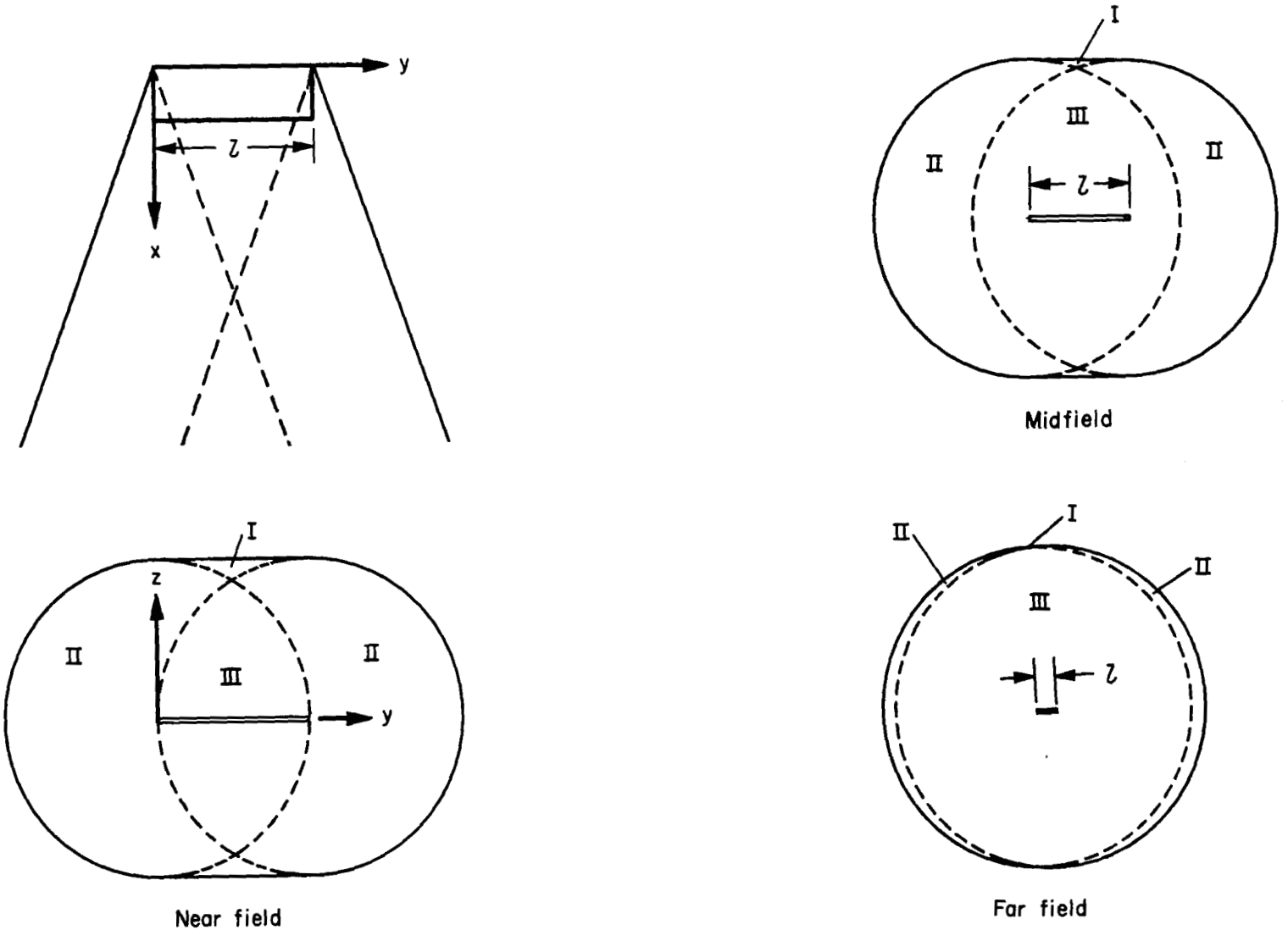

Figure 1.– Coordinate system and wave geometry for the rectangular wing.

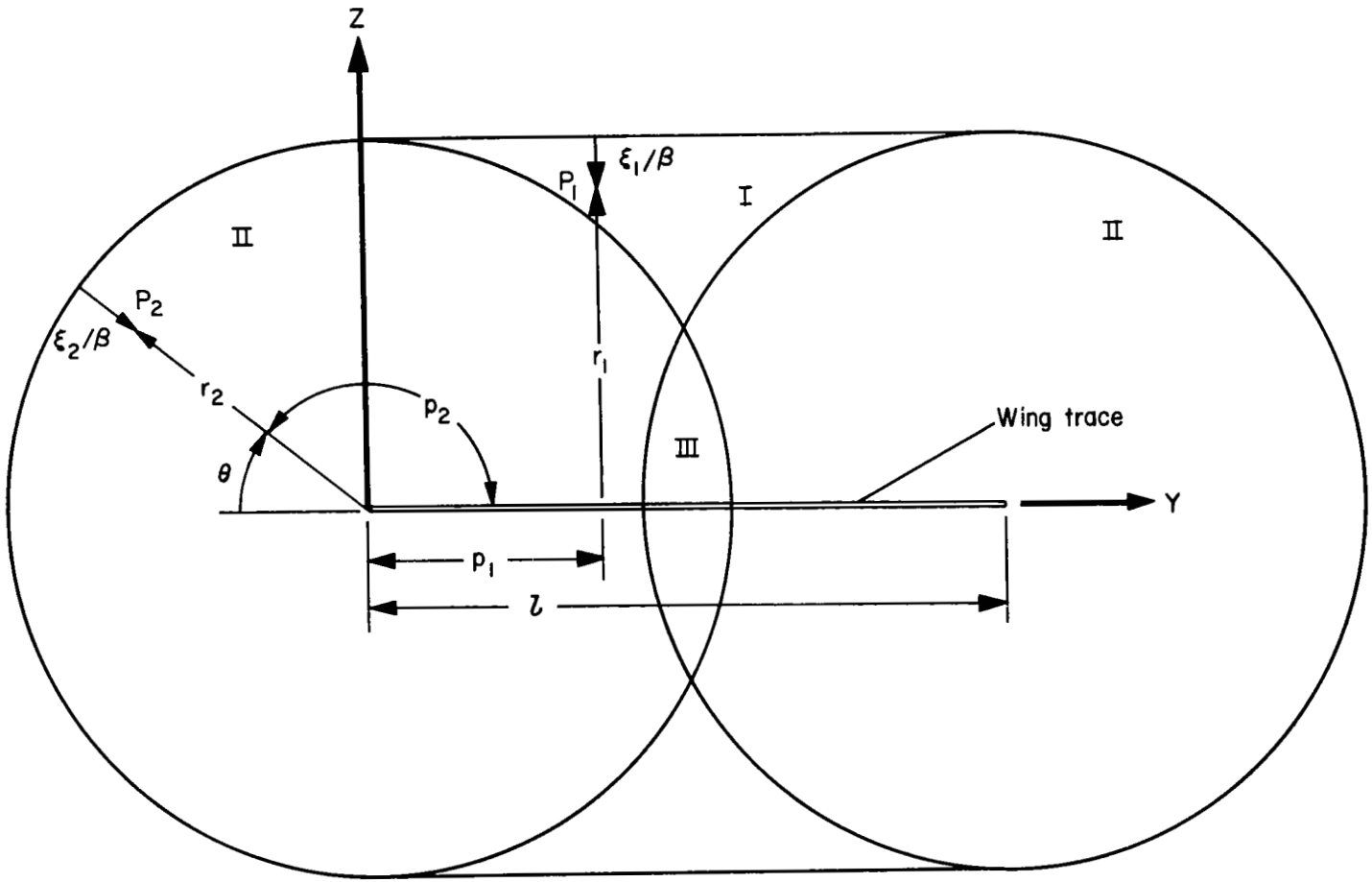

Figure 2.– Wave front pattern and transformed coordinates in a plane x = constant.

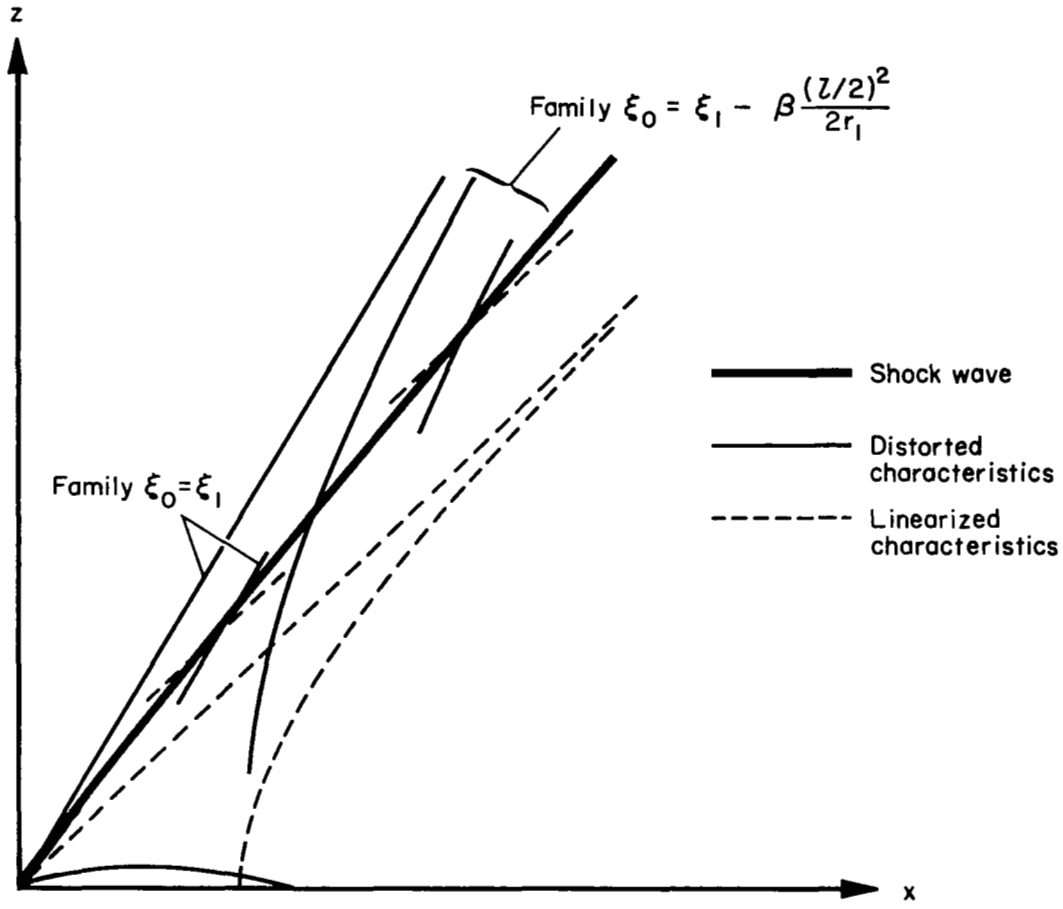

Figure 3.– Shock wave and distorted characteristics in the plane $p_1 = (1/2)l$.

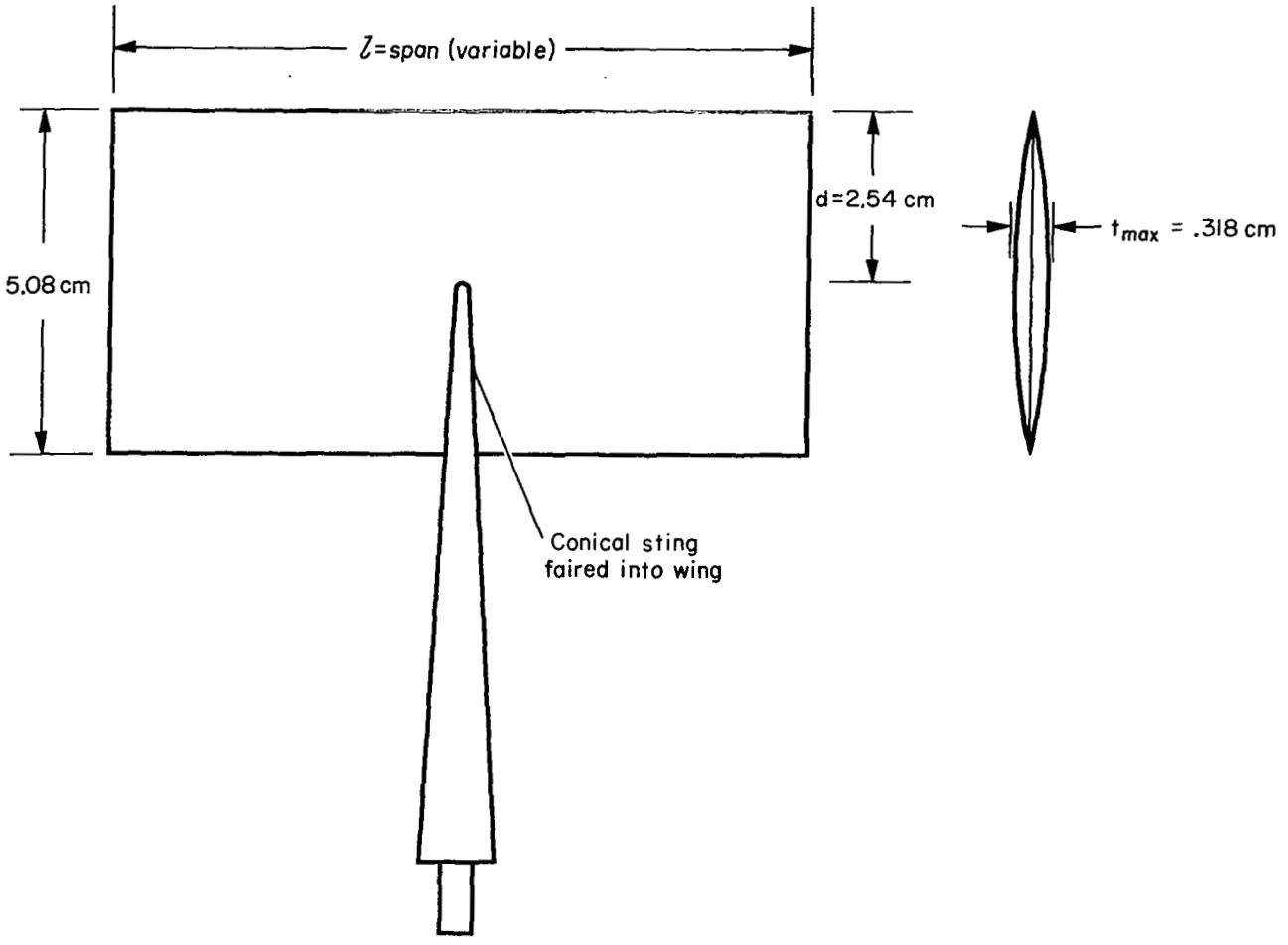

Figure 4.– Rectangular wing model (1095 tool steel).

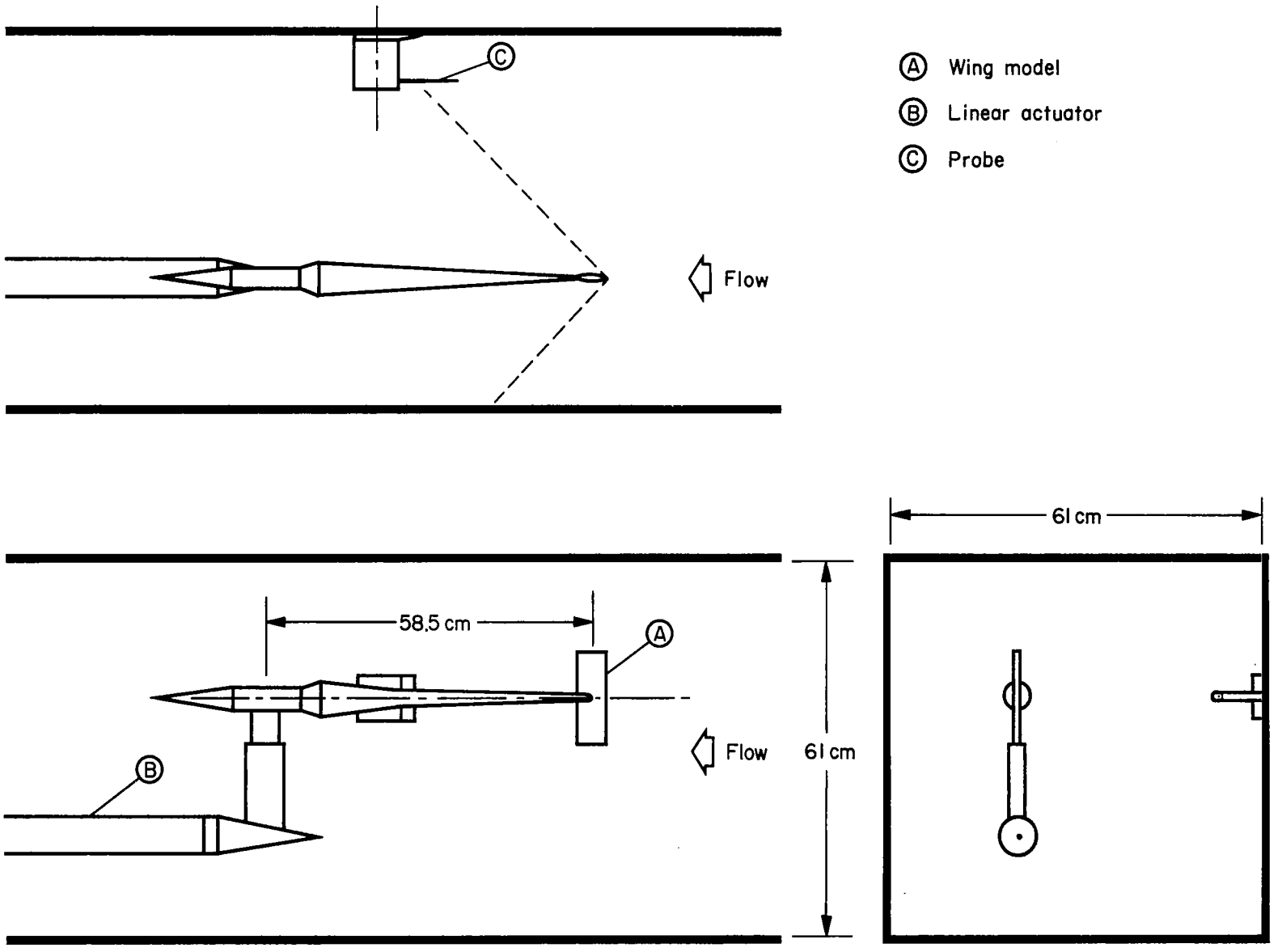

Figure 5.– Test configuration in 2- by 2-foot wind tunnel.

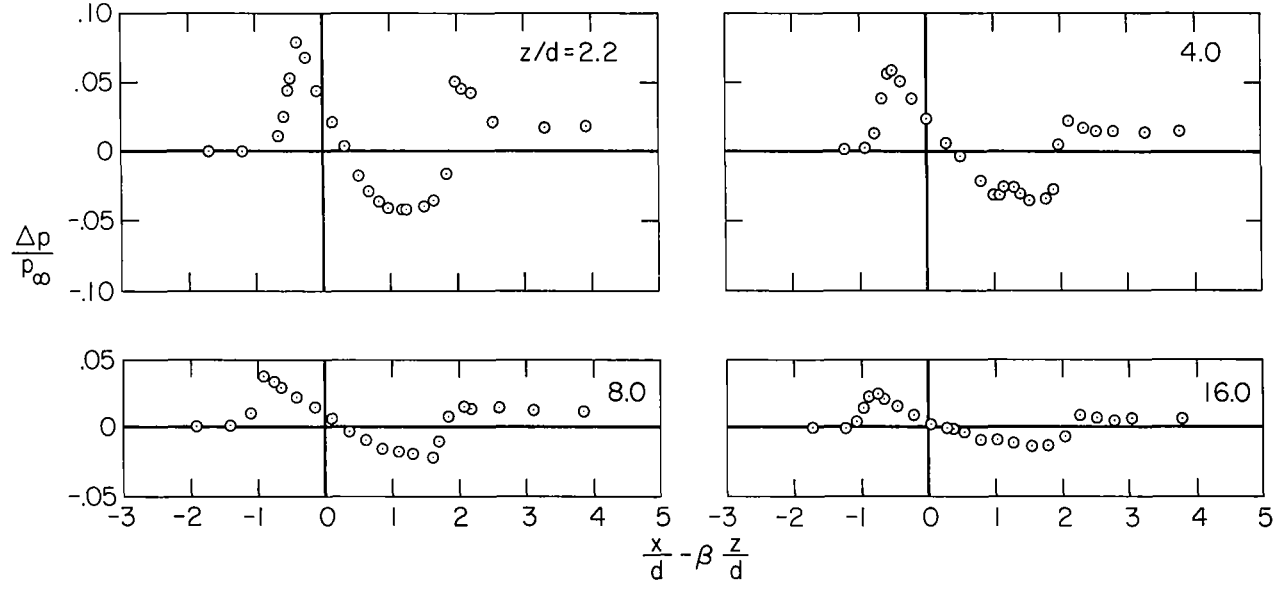

(a) $\ell/d = 1$

Figure 6.– Effect of distance on the shock-wave signature measured in the plane of symmetry, M = 1.4.

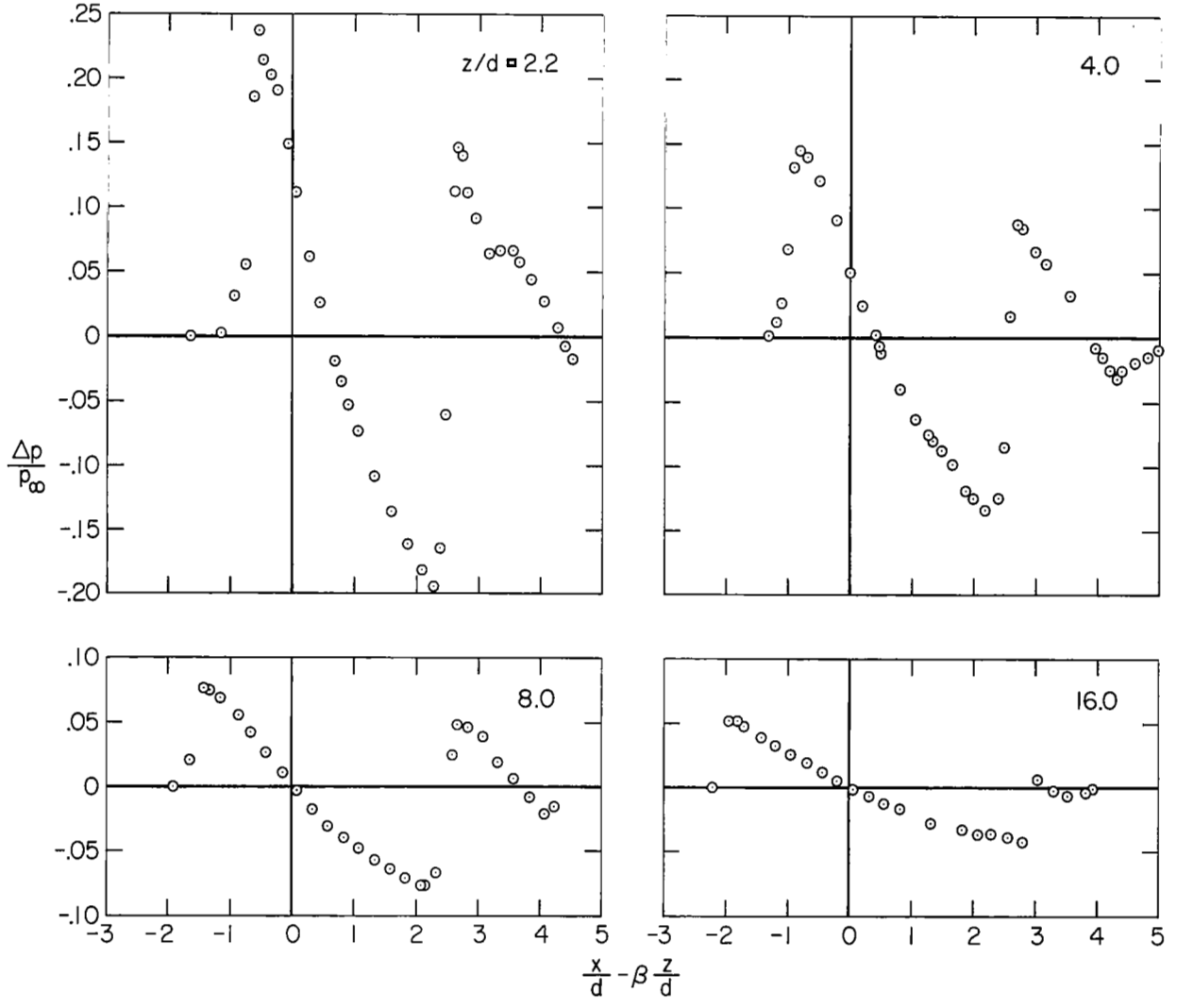

(b) $z/d = 4$

Figure 6.– Continued.

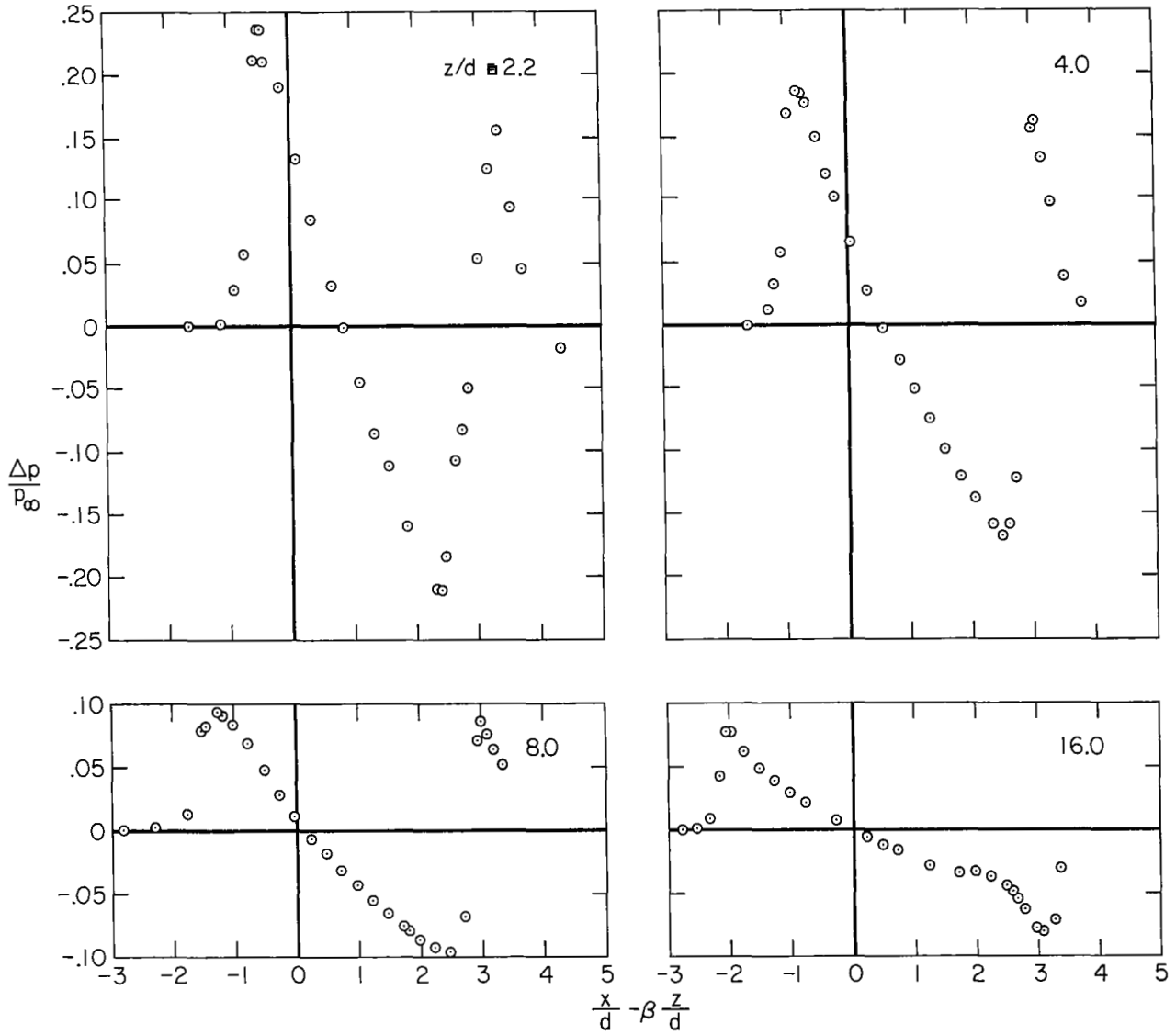

(c) $\ell/d = 6$

Figure 6.– Concluded.

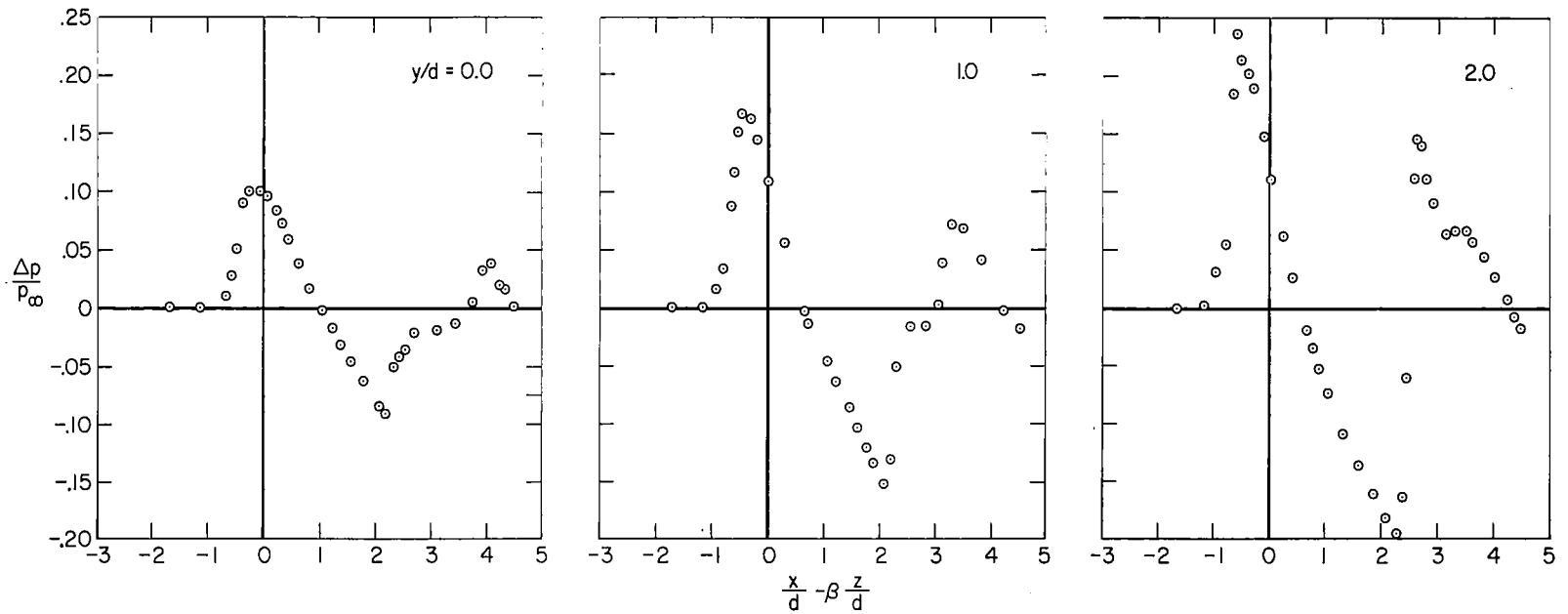

(a) z/d = 2.2

Figure 7.– Shock-wave signatures measured at several spanwise stations; $\ell/d = 4$, M = 1.4.

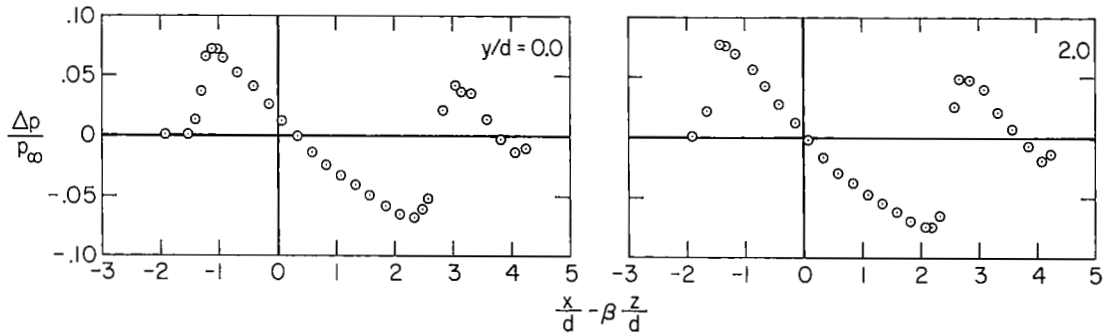

(b) z/d = 8

Figure 7.– Concluded.

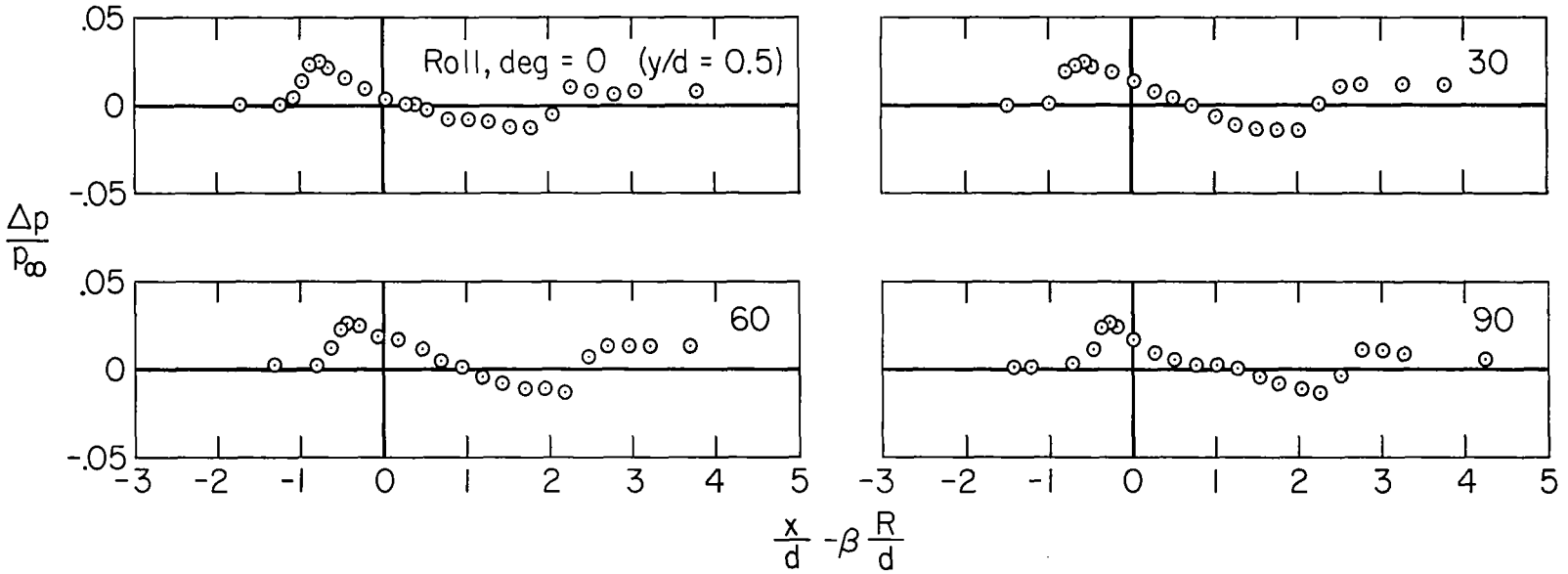

(a) $\ell/d = 1$

Figure 8.– Effect of roll on the shock-wave signatures; R/d = 16, M = 1.4.

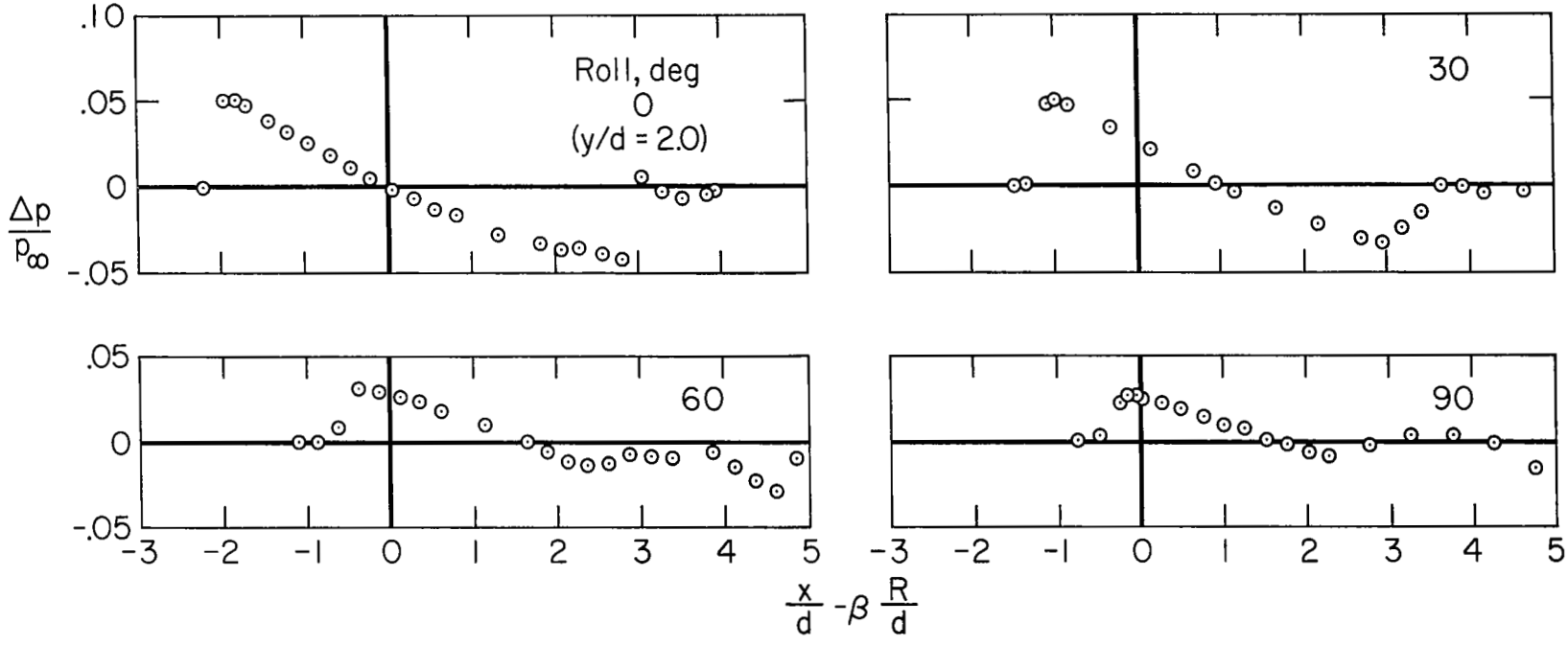

(b) $\ell/d = 4$

Figure 8.– Continued.

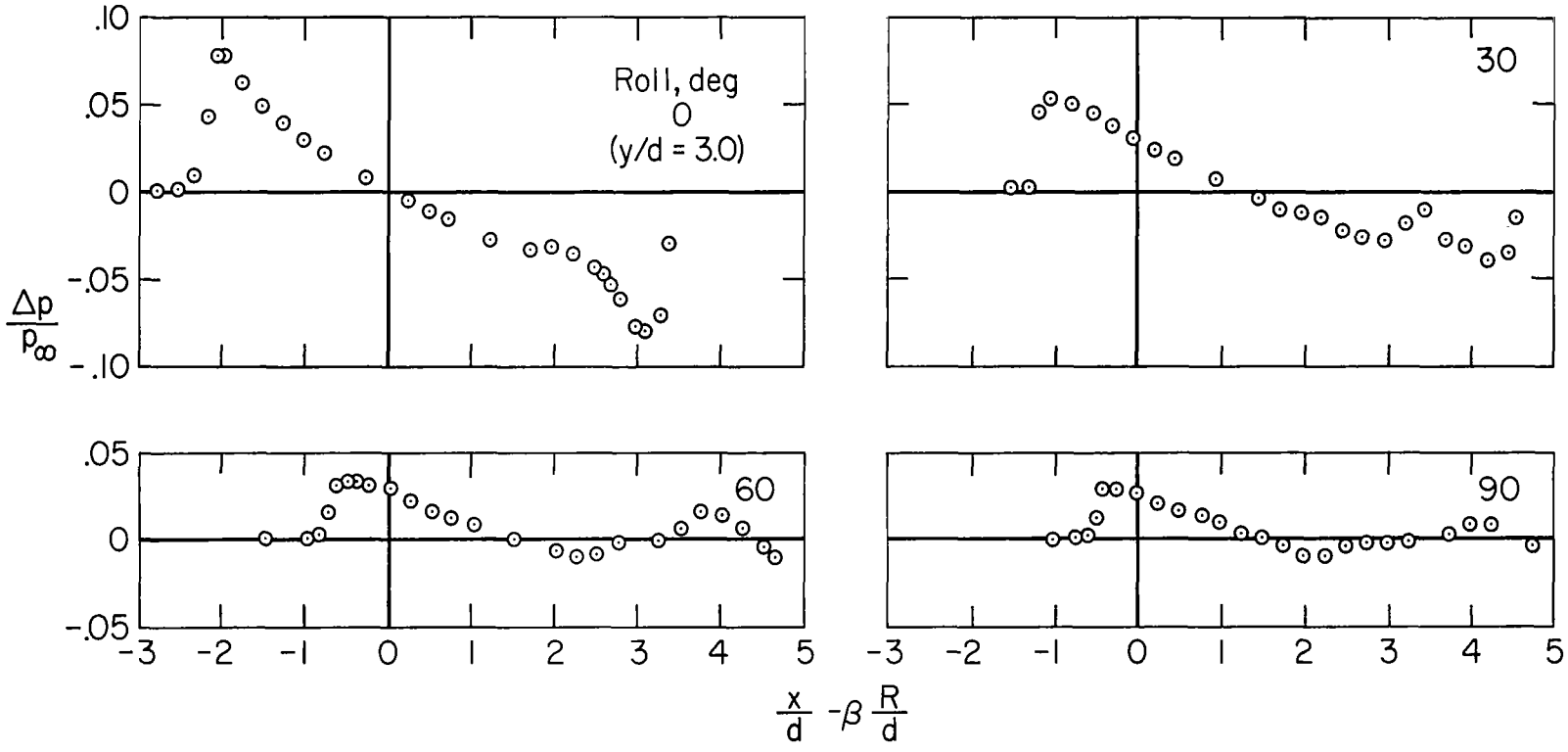

(c) $\ell/d = 6$

Figure 8.– Concluded.

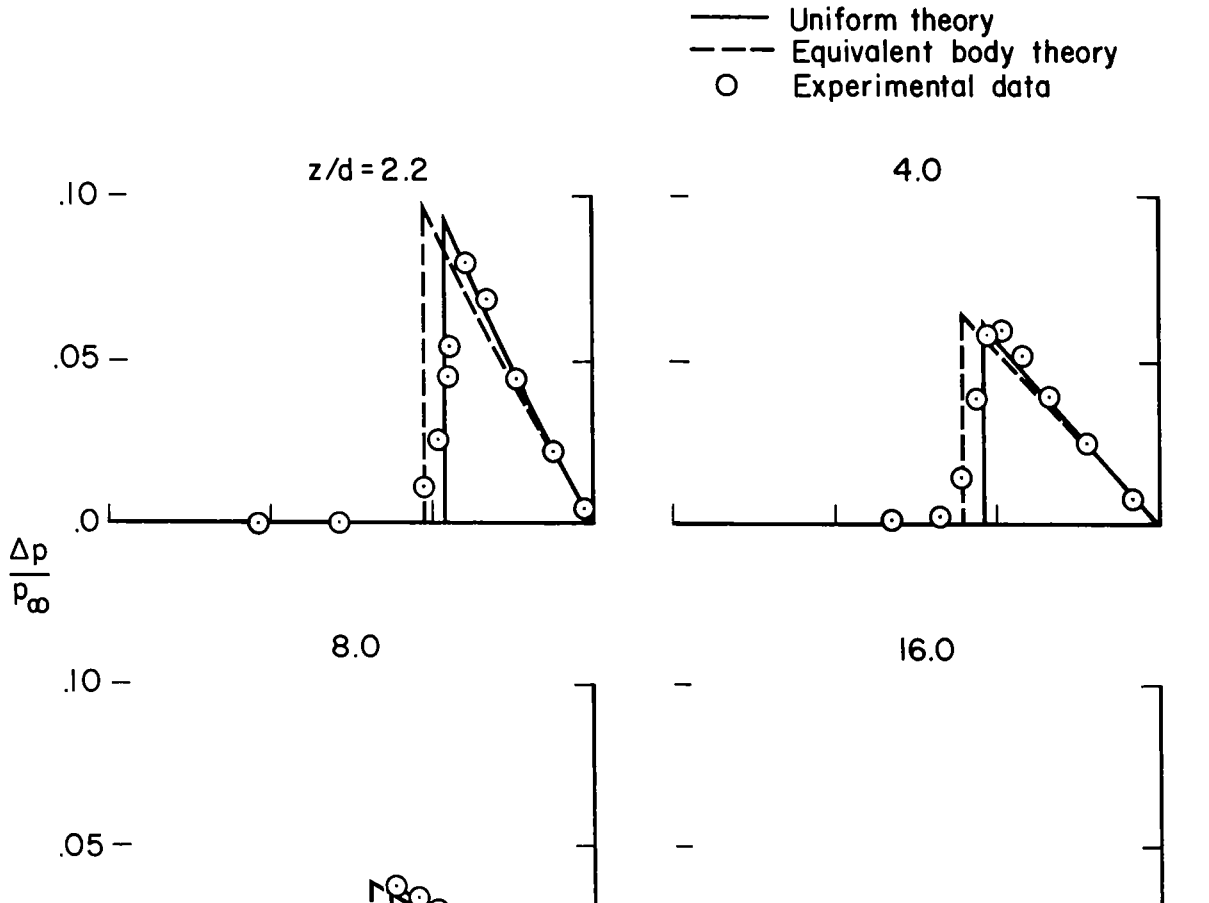

(a) $\ell/d = 1$

Figure 9.– Comparison of uniform theory, equivalent body theory, and experiment for the overpressure signature in the plane of symmetry, M = 1.4.

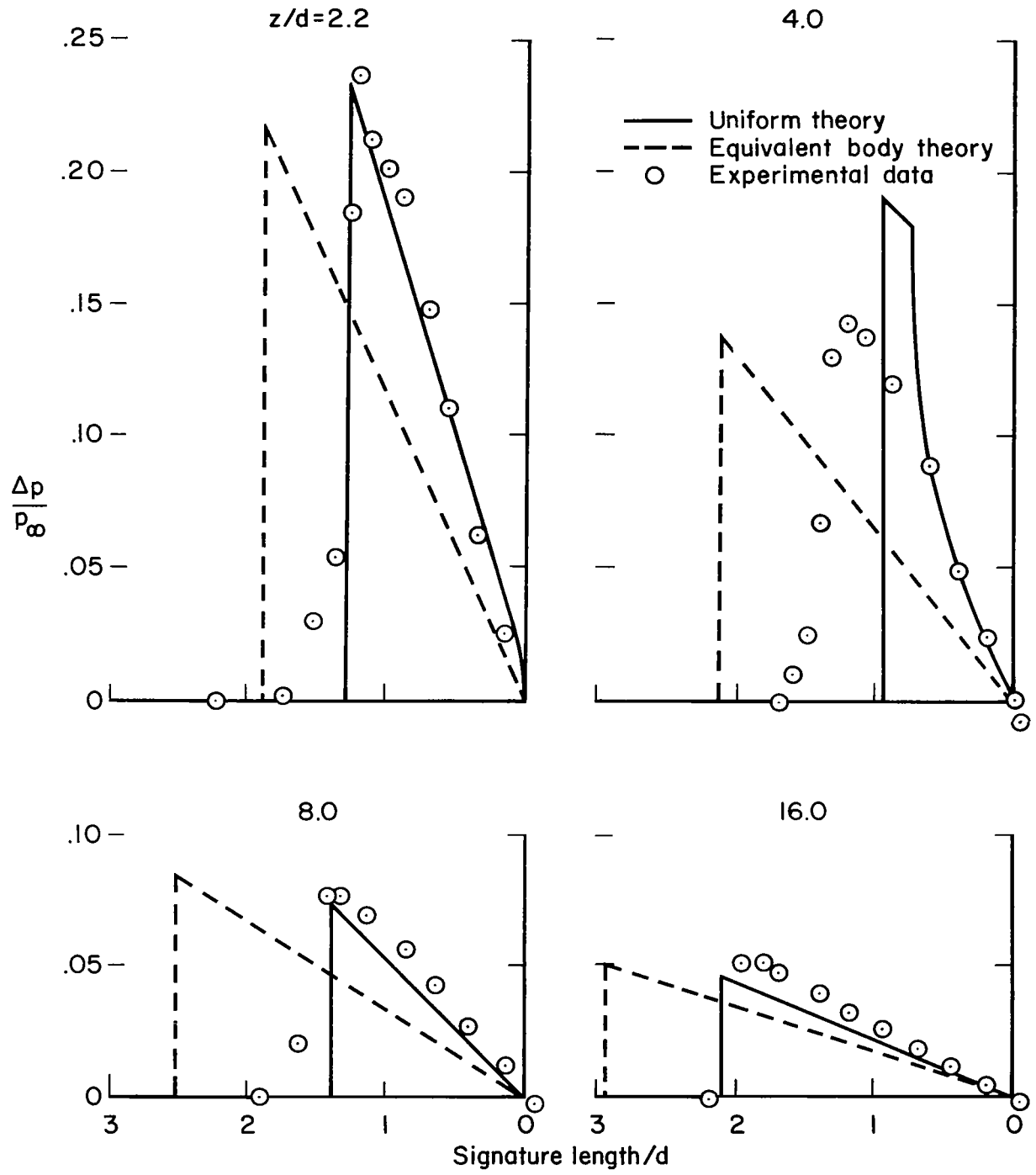

(b) $\ell/d = 4$

Figure 9.– Continued.

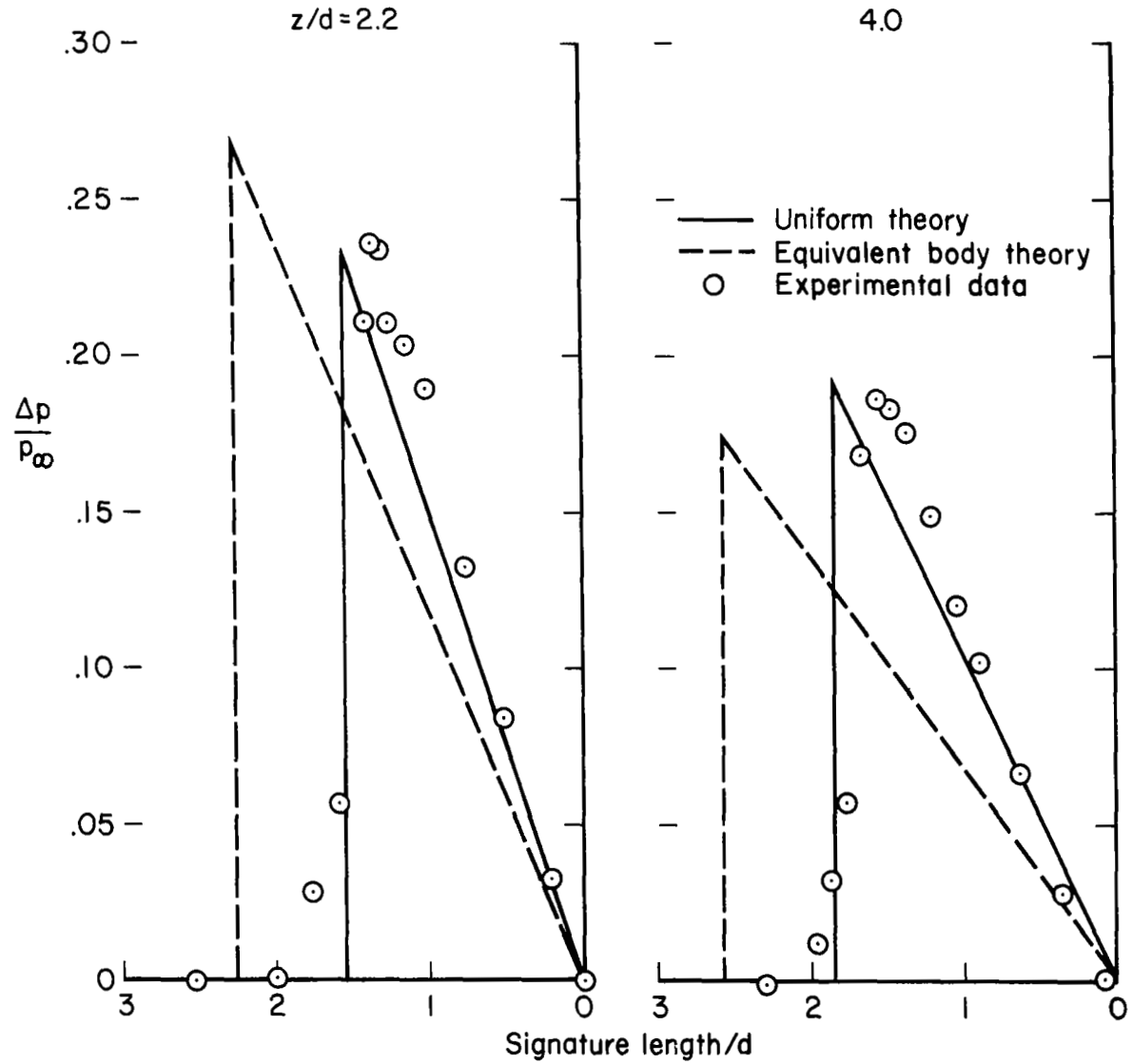

(c) $\ell/d = 6$

Figure 9.– Continued.

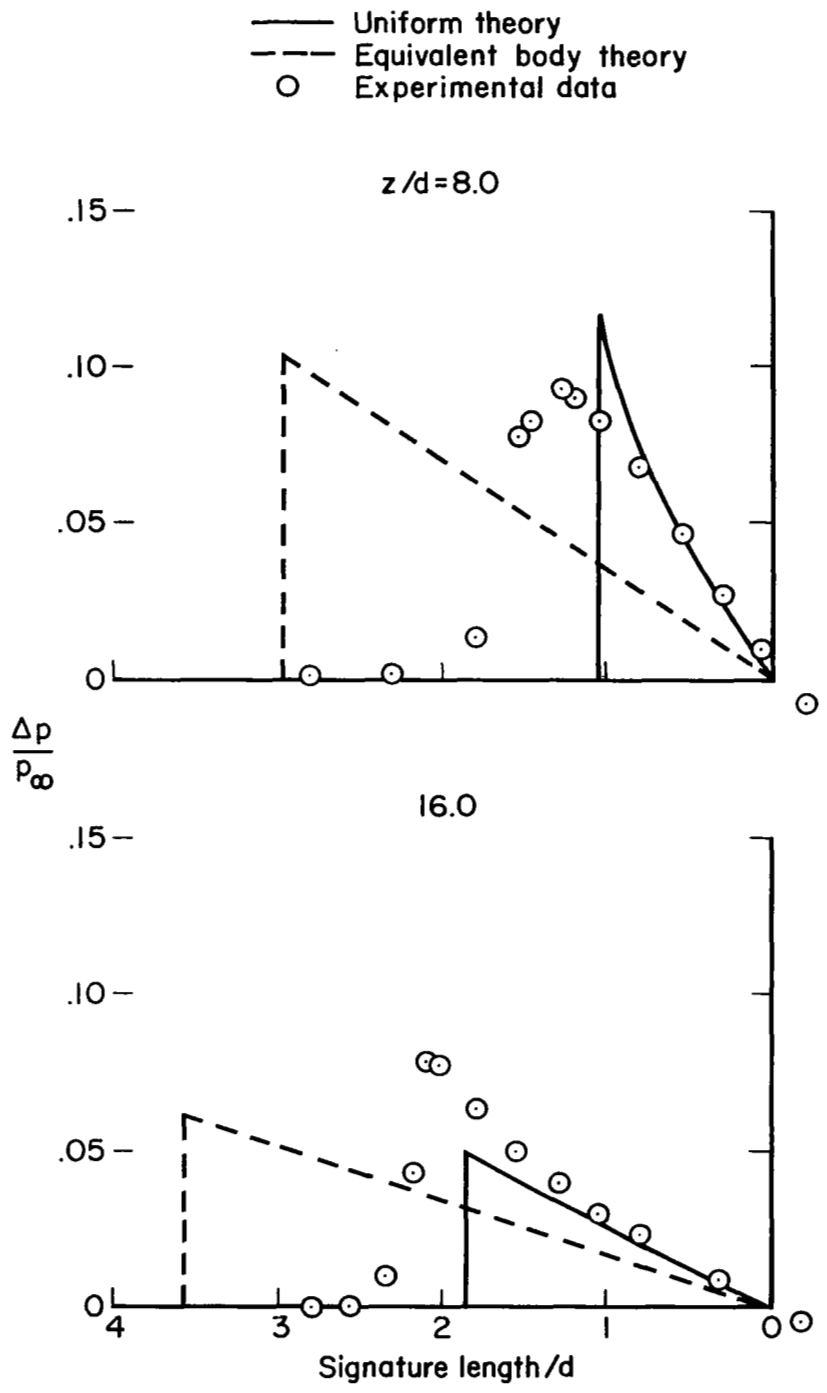

(c) $\ell/d = 6$ – Concluded.

Figure 9.– Concluded.

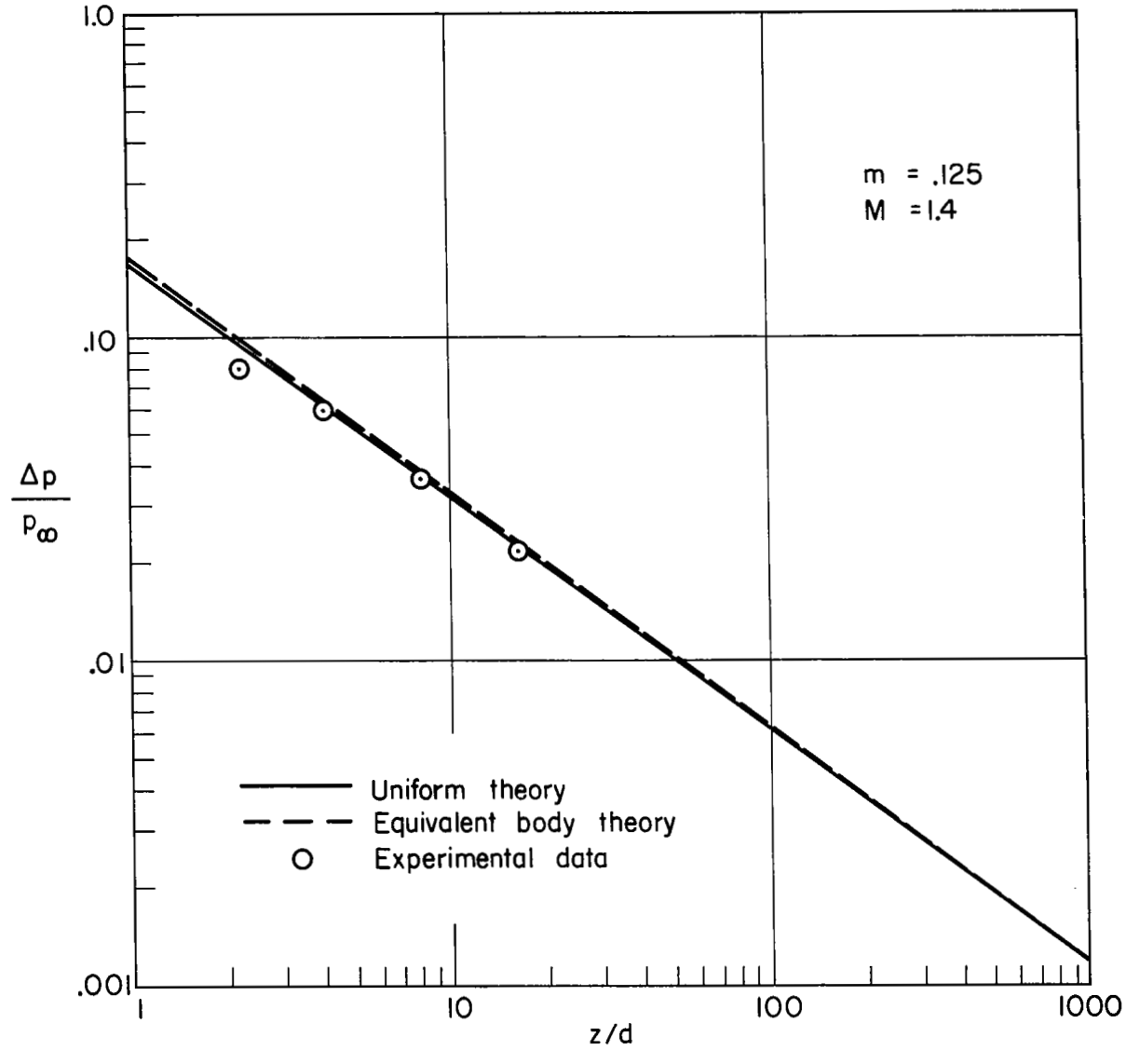

(a) $\ell/d = 1$

Figure 10.– Decay of peak pressure rise with distance below wing.

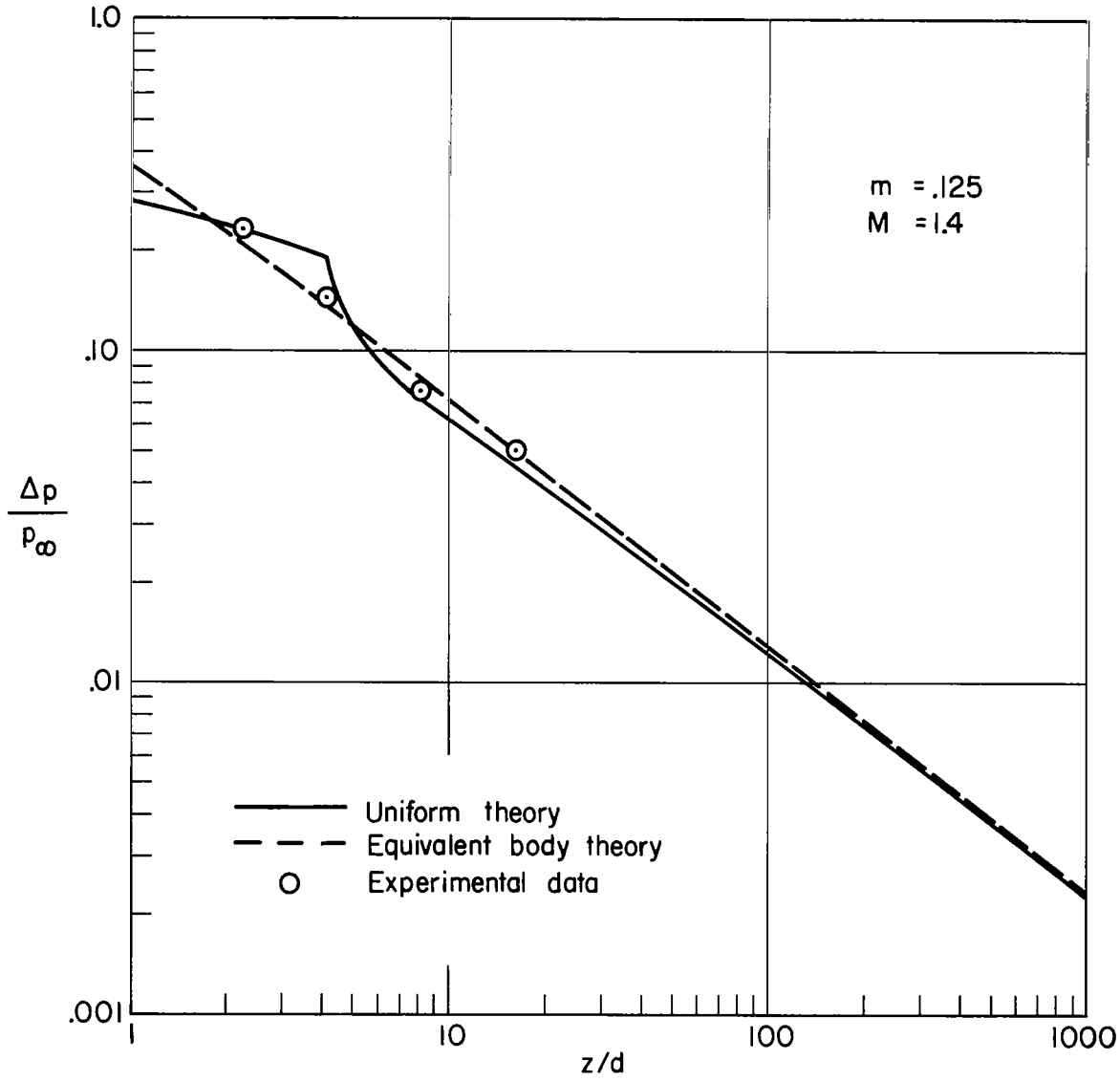

(b) $\ell/d = 4$

Figure 10.– Continued.

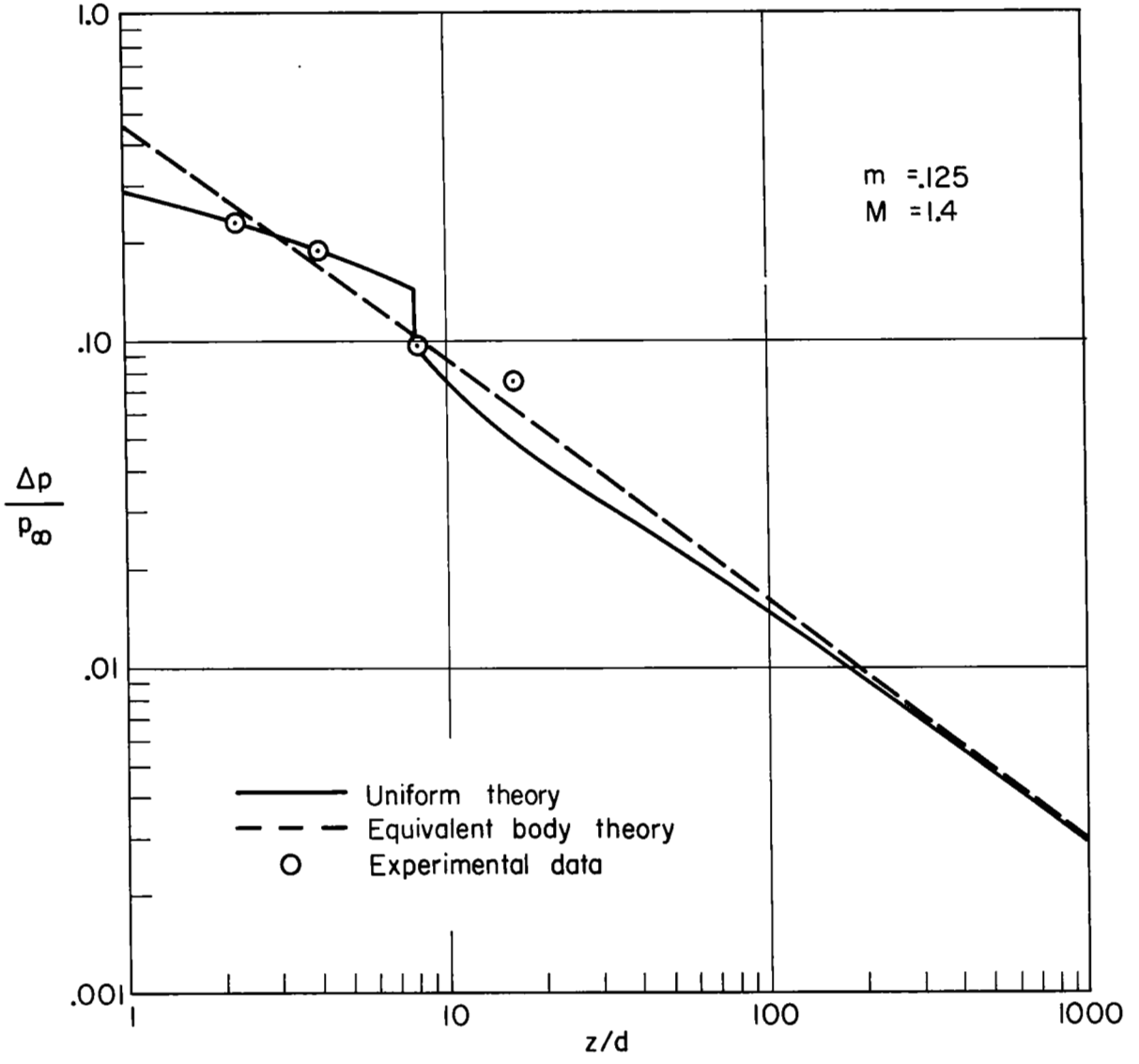

(c) $\ell/d = 6$

Figure 10.– Concluded.

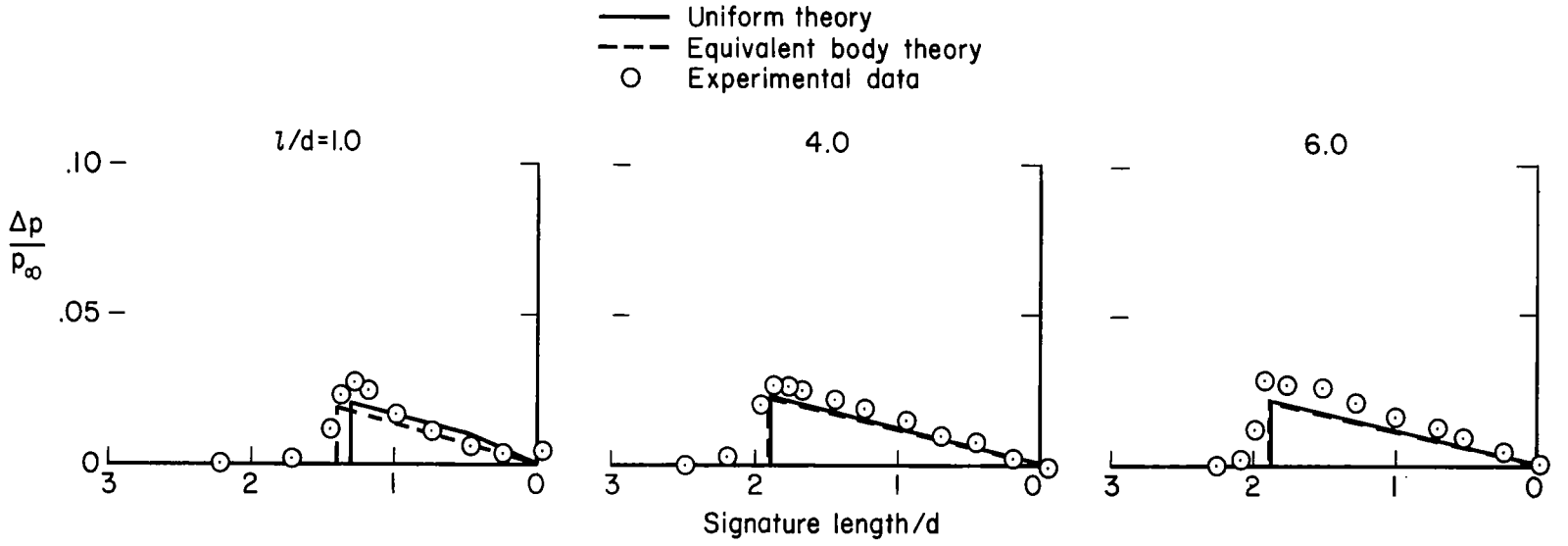

Figure 11.– Overpressure signatures measured at R/d = 16.0 for a roll angle about the axis of symmetry of 90°, M = 1.4.

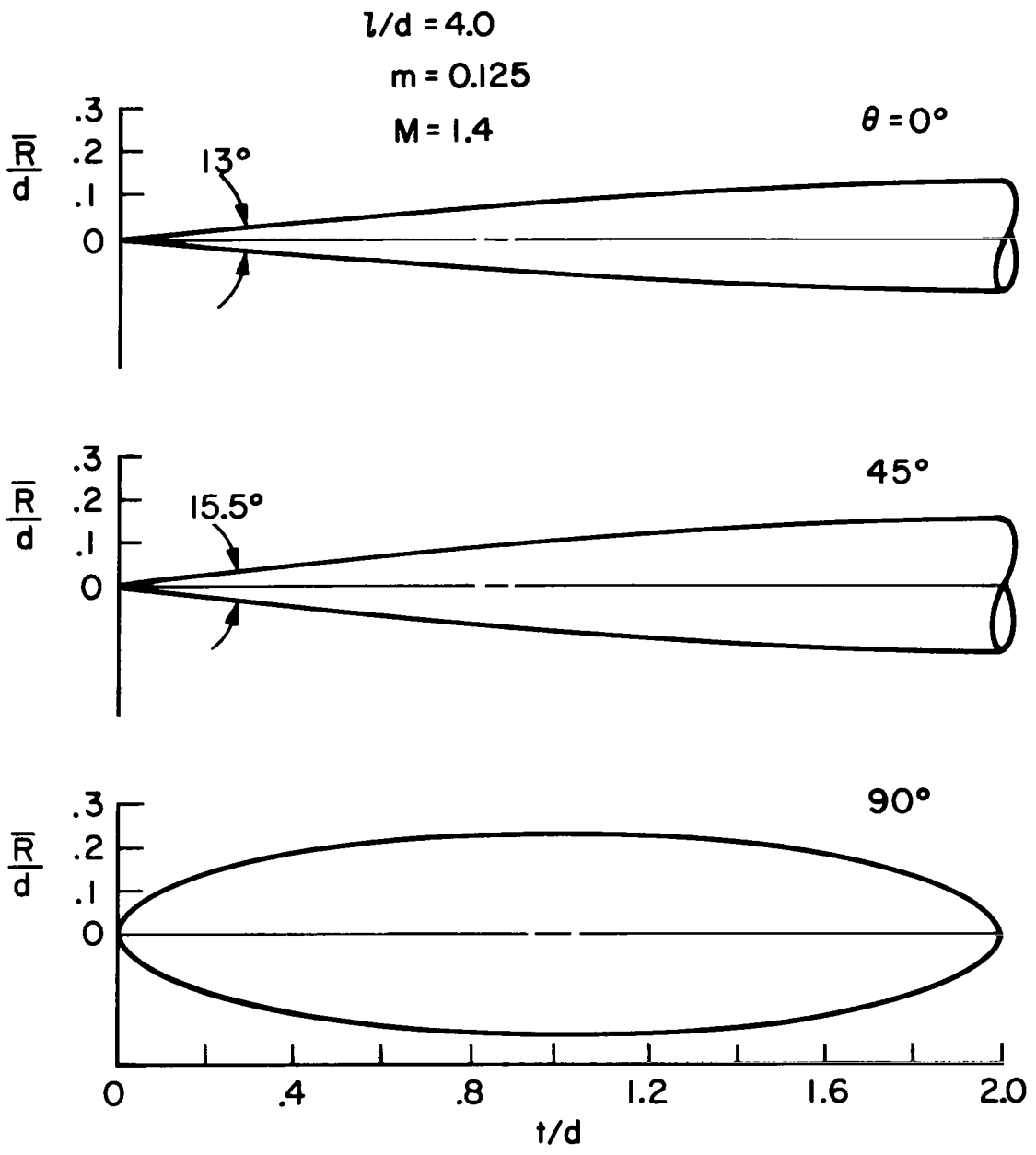

Figure 12.– Equivalent body of revolution for the rectangular wing.

NASA-Langley, 1971 — 2 A-4109

017 001 C1 U 02 711124 S00903DS
DEPT OF THE AIR FORCE
AF WEAPONS LAB (AFSC)
TECH LIBRARY/WLOL/
ATTN: E LOU BOWMAN, CHIEF
KIRTLAND AFB NM 87117

"The aeronautical and space activities of the United States shall be conducted so as to contribute . . . to the expansion of human knowledge of phenomena in the atmosphere and space. The Administration shall provide for the widest practicable and appropriate dissemination of information concerning its activities and the results thereof."

—NATIONAL AERONAUTICS AND SPACE ACT OF 1958

NASA SCIENTIFIC AND TECHNICAL PUBLICATIONS

TECHNICAL REPORTS: Scientific and technical information considered important, complete, and a lasting contribution to existing knowledge.

TECHNICAL NOTES: Information less broad in scope but nevertheless of importance as a contribution to existing knowledge.

TECHNICAL MEMORANDUMS: Information receiving limited distribution because of preliminary data, security classification, or other reasons.

CONTRACTOR REPORTS: Scientific and technical information generated under a NASA contract or grant and considered an important contribution to existing knowledge.

TECHNICAL TRANSLATIONS: Information published in a foreign language considered to merit NASA distribution in English.

SPECIAL PUBLICATIONS: Information derived from or of value to NASA activities. Publications include conference proceedings, monographs, data compilations, handbooks, sourcebooks, and special bibliographies.

TECHNOLOGY UTILIZATION PUBLICATIONS: Information on technology used by NASA that may be of particular interest in commercial and other non-aerospace applications. Publications include Tech Briefs, Technology Utilization Reports and Technology Surveys.

Details on the availability of these publications may be obtained from:

SCIENTIFIC AND TECHNICAL INFORMATION OFFICE

NATIONAL AERONAUTICS AND SPACE ADMINISTRATION

Washington, D.C. 20546